JGR Oceans

RESEARCH ARTICLE
10.1029/2023JC019947

Special Section:
Physical and biogeochemical processes affecting nutrients and the carbon cycle in mesoscale eddies of subtropical oceans

Enhanced Phosphate Consumption Stimulated by Nitrogen Fixation Within a Cyclonic Eddy in the Northwest Pacific

Zhongwei Yuan[1,2], Thomas J. Browning[2], Chuanjun Du[3], Hui Shen[1], Lei Wang[4], Yifan Ma[1], Zong-Pei Jiang[5], Zhiyu Liu[1], Kuanbo Zhou[1], Shuh-Ji Kao[1], and Minhan Dai[1]

[1]State Key Laboratory of Marine Environmental Science & College of Ocean and Earth Sciences, Xiamen University, Xiamen, China, [2]Marine Biogeochemistry Division, GEOMAR Helmholtz Centre for Ocean Research, Kiel, Germany, [3]State Key Laboratory of Marine Resource Utilization in South China Sea, Hainan University, Haikou, China, [4]Third Institute of Oceanography, Ministry of Natural Resources, Xiamen, China, [5]Ocean College, Zhejiang University, Zhoushan, China

Abstract Mesoscale eddies are common in the subtropical Northwest Pacific, however, relatively little is known about their spatial variability and temporal evolution, and how these impact upper ocean biogeochemistry. Here we investigate these using observations of a cyclonic eddy carried out along four sequential transects. Consistent with previous observations of cyclonic eddies, the eddy core had doming isopycnals, bringing elevated nutrient waters nearer to the surface. However, we also found that the upper layer of the eddy above the nutricline had significantly lower phosphate concentrations within its core relative to its edge. We attributed this to elevated N_2 fixation within the eddy core, which was likely driven by enhanced subsurface iron supply, ultimately resulting in increased phosphate consumption. Eddy-enhanced N_2 fixation was additionally supported by the elevation of nitrate + nitrite to phosphate ratios below the euphotic zone. Moreover, we observed that while the upward displacement of isopycnals within the eddy core led to an increase in phytoplankton biomass in the lower euphotic zone, there was no significant increase in total phytoplankton biomass across the entire euphotic zone. Cyclonic eddies in the subtropical North Pacific are projected to be becoming more frequent, implying that such dynamics could become increasingly important for regulating nutrient biogeochemistry and ultimately productivity of the region.

Plain Language Summary Cyclonic eddies are oceanographic features leading to upward transfer of deep-water nutrients that support phytoplankton growth in the sunlit surface ocean. In the low-nutrient Northwest Pacific, cyclonic eddies are considered to be an extremely important nutrient source in alleviating nutrient limitation; however, their biogeochemical effects are not well-examined, in particular in the upper layers where nutrients are below the detection limit of conventional techniques. By examining a cyclonic eddy with four sequential transect observations, our results showed that the eddy core had higher nutrient concentrations in the lower euphotic zone compared to the eddy edge, consistent with previous studies; in contrast, concentrations of phosphate in the upper surface layer had significantly lower values within the core relative to those at the edge. Surface rate measurements suggested that this lower phosphate was potentially driven by elevated N_2 fixation, likely due to enhanced iron supply from depth, thereby resulting in additional consumption of excess surface phosphate. However, this increased nutrient supply did not lead to the enhancement of total phytoplankton biomass across the entire euphotic zone.

Key Points:

- Lower phosphate concentrations were observed above the nutricline within the eddy core in comparison to the edge
- Enhanced N_2 fixation within the eddy core is proposed to have driven increased phosphate consumption
- No substantial total phytoplankton biomass increase was found within the eddy core

Supporting Information:

Supporting Information may be found in the online version of this article.

Correspondence to:
M. Dai,
mdai@xmu.edu.cn

Citation:
Yuan, Z., Browning, T. J., Du, C., Shen, H., Wang, L., Ma, Y., et al. (2023). Enhanced phosphate consumption stimulated by nitrogen fixation within a cyclonic eddy in the Northwest Pacific. *Journal of Geophysical Research: Oceans*, *128*, e2023JC019947. https://doi.org/10.1029/2023JC019947

Received 19 APR 2023
Accepted 11 OCT 2023

Author Contributions:

Conceptualization: Zhongwei Yuan, Thomas J. Browning, Kuanbo Zhou, Minhan Dai
Data curation: Zhongwei Yuan, Lei Wang, Zhiyu Liu, Shuh-Ji Kao, Minhan Dai
Formal analysis: Zhongwei Yuan
Funding acquisition: Kuanbo Zhou, Minhan Dai
Investigation: Zhongwei Yuan, Chuanjun Du, Hui Shen, Yifan Ma, Zong-Pei Jiang
Methodology: Zhongwei Yuan
Project Administration: Minhan Dai
Resources: Zhongwei Yuan, Minhan Dai
Software: Zhongwei Yuan

1. Introduction

The biological pump, which sequesters carbon into the deeper ocean via sinking particles, concomitantly removes nutrients from the surface ocean (Ducklow et al., 2001). This can draw down nutrients to levels limiting phytoplankton growth (Moore et al., 2013). Processes of vertical diapycnal mixing, vertical and lateral advection, N_2 fixation and atmospheric nutrient deposition collectively resupply nutrients to the surface ocean (Duce et al., 2008; Karl et al., 1997; Letscher et al., 2016; Lewis et al., 1986). Episodic features, such as those regulated by mesoscale cyclonic eddies, may form a vital constituent of the annual nutrient supply, probably contributing to >20% of the nitrogen (N) requirement to support observed global new production—the fraction of primary production fueled by newly supplied N (Garçon et al., 2001; Johnson et al., 2010; McGillicuddy & Robinson, 1997; McGillicuddy et al., 1998, 2007; Oschlies & Garçon, 1998).

Supervision: Thomas J. Browning, Minhan Dai
Validation: Zhongwei Yuan, Thomas J. Browning
Visualization: Zhongwei Yuan
Writing – original draft: Zhongwei Yuan
Writing – review & editing: Zhongwei Yuan, Thomas J. Browning, Chuanjun Du, Minhan Dai

Mesoscale cyclonic eddies with radius scales on the order of 100 km are ubiquitous features of the open ocean (Chaigneau et al., 2009; Chelton, Schlax, & Samelson, 2011). These features shoal the thermocline, thereby influencing nutrient availability and subsequent phytoplankton community responses in the upper ocean (e.g., Barone et al., 2022; Benitez-Nelson et al., 2007; Falkowski et al., 1991; Hawco et al., 2021; McGillicuddy et al., 1998, 2007; Zhou et al., 2023). Previous studies of the biogeochemical impacts of cyclonic eddies tended to focus on either comparing the difference within (where the maximum vertical isopycnal displacement occurred) and outside one specific eddy (Allen et al., 1996; Benitez-Nelson et al., 2007; Brown et al., 2008; Browning et al., 2021; Q. P. Li & Hansell, 2008; Vaillancourt et al., 2003), or contrasting between different eddies (Barone et al., 2022; Dufois et al., 2016; Dugenne et al., 2023; Guidi et al., 2012; McGillicuddy et al., 2007; Rii et al., 2008; Seki et al., 2001; Yun et al., 2020; Zhou et al., 2020, 2023). It has been proposed that submesoscale structures (i.e., oceanic motions with spatial scales of 0.2–20 km) within eddies, such as spiral bands, could supply more nutrients compared with when only larger-scale processes are considered (Klein & Lapeyre, 2009; Z. Zhang & Qiu, 2020). Additionally, cyclonic eddies at different developmental phases, such as intensification (i.e., nutrient injection into the euphotic zone stimulates a biological response), mature (i.e., a cyclone attains its maximum tangential velocity, production rate, and highest biomass), and decay (i.e., the doming of the isopycnals relaxes and tangential velocity decreases), would also shape variable intensity in nutrient injection and subsequent differences in biological community composition (Rii et al., 2008; Sweeney et al., 2003). To date, however, the effects of spatial variability along with eddy evolution on upper ocean biogeochemistry within cyclonic eddies remain poorly understood, due partly to their ephemeral nature and undersampling.

The subtropical Northwest Pacific, characterized by low nutrients and low phytoplankton biomass (Dai et al., 2023; Martiny et al., 2019), is increasingly impacted by eddies (Chelton, Schlax, & Samelson, 2011; Y. Liu et al., 2012; Qiu & Chen, 2010). Accordingly, upwelling of deep waters in this region via cyclonic eddies could facilitate an enhanced nutrient supply into the euphotic zone, potentially temporarily alleviating limitations on bulk phytoplankton growth imposed by N, phosphorus (P), and/or iron (Fe) availability (Browning et al., 2022; Q. Li et al., 2015; Moore et al., 2013; Yuan et al., 2023). This process may additionally impact the growth of N_2-fixing microorganisms (diazotrophs) owing to the altered supply rate of N relative to that of Fe (Ward et al., 2013; Wen et al., 2022). In this context, we performed a comprehensive investigation of a cyclonic eddy in the subtropical Northwest Pacific, with four sequential transect observations to determine the spatio-temporal variabilities of the upper ocean biogeochemistry.

2. Materials and Methods

2.1. General

Fieldwork was conducted onboard RV Tan Kah Kee in the early spring from 15 March to 20 April 2019 (project "SILICON") in the western oligotrophic North Pacific (surface chlorophyll *a* 0.03–0.07 mg m^{-3}; Figure 1a). The targeted cyclonic eddy, denoted as Eddy E2, with an approximate diameter of ~200 km, was tracked and repeatedly sampled across four zonal transects (transects termed E2-1, E2-2, E2-3, and E2-4, respectively). Discrete depth profile samples for nutrients and Dissolved oxygen (DO) were collected at 10 m vertical intervals throughout the upper 200 m, followed by 300, 400, and 500 m, using 12-L Niskin sampling bottles alongside a conductivity-temperature-depth (CTD) profiler. The mixed layer depth (MLD) was calculated using the threshold method of de Boyer Montégut et al. (2004). Here, the MLD is determined as the depth where a density difference of 0.125 kg m^{-3} from that at a 10 m reference depth is reached. The photosynthetically active radiation (PAR) sensor attached to the CTD was used to identify the euphotic zone (here defined as the 0.1% surface PAR, Z_{eu}; Table 1). A significant correlation between the depth of Z_{eu} (those collected during daytime) and the depth of deep chlorophyll maximum (DCM) was observed ($Z_{eu} = 0.47 \times DCM + 99.95$, $R^2 = 0.55$, $n = 19$, $p < 0.001$). The depths of Z_{eu}, where PAR was not measured, were then estimated using this relationship (Table 1). The altimetric Mesoscale Eddy Trajectory Atlas products were extracted from the AVISO+ website (https://data.aviso.altimetry.fr/aviso-gateway/data/META3.1exp_DT/META3.1exp_DT_allsat/). Daily sea level anomaly (SLA) at 0.25° resolution based on satellite altimetry measurements was obtained from the Copernicus Climate Data Store (https://cds.climate.copernicus.eu/). The satellite-derived chlorophyll *a* for April 2019 at 9 km resolution was downloaded from the NASA Ocean Color website (standard MODIS-Aqua L3 product, https://oceancolor.gsfc.nasa.gov).

2.2. Nutrients and Dissolved Oxygen

Nutrient samples (nitrate plus nitrite, N + N; phosphate; silicate) were collected in acid-washed Nalgene HDPE bottles and immediately measured colorimetrically onboard using a Four-channel Continuous Flow Technicon

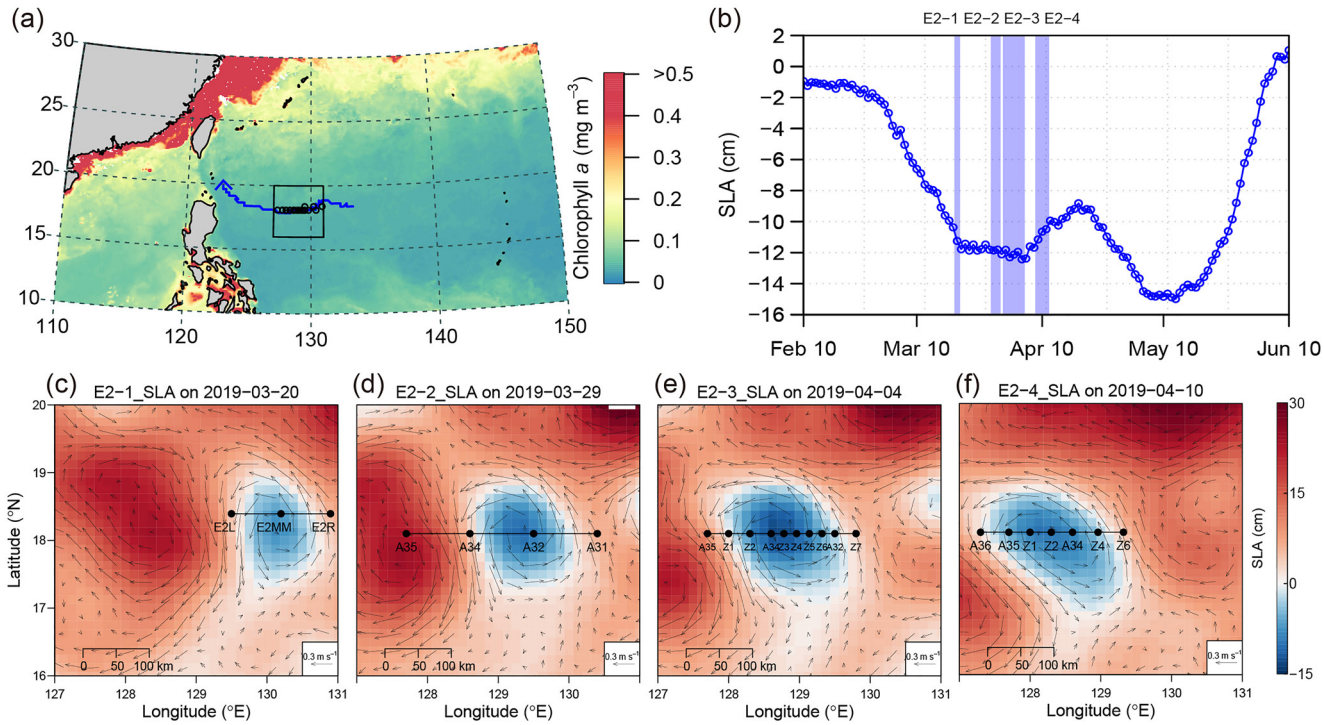

Figure 1. Study area and the evolution of Eddy E2. (a) Map of the western North Pacific showing the sampling locations (open circles) with the context of satellite-derived chlorophyll *a* in April 2019. Blue line indicates the trajectory of the center of Eddy E2 within the whole lifespan. Boxed regions identify the study locations. (b) Sea level anomaly (SLA) of the center of Eddy E2 within the whole lifespan. The shaded bars indicate the periods of four observations. (c–f) Surface distribution of SLA and the satellite-derived geostrophic current velocities corresponding to the date when sampling campaigns were conducted at the eddy core. Black dots represent the sampling stations along the transects.

AA3 Auto-Analyzer (Bran-Lube GmbH) (Han et al., 2012). The concentration of nitrate was then determined by subtraction ($[NO_3^-] = [N + N] - [\text{nitrite}]$). The detection limits for nitrate (NO_3^-), nitrite (NO_2^-), phosphate (PO_4^{3-}), and silicate ($Si(OH)_4$) were 0.03, 0.02, 0.03, and 0.05 μmol L^{-1}, respectively, and the analytical precisions (repeat measurements of aged deep seawater) were 0.9% for NO_3^- (38.28 ± 0.35 μmol L^{-1}, mean ± s.d., $n = 56$), 52.3% for NO_2^- (0.065 ± 0.034 μmol L^{-1}, $n = 56$), 1.7% for PO_4^{3-} (2.749 ± 0.047 μmol L^{-1}, $n = 56$), and 0.5% for $Si(OH)_4$ (148.4 ± 0.8 μmol L^{-1}, $n = 56$). Certified reference materials Lot. BZ and Lot. CB (RMNS; KANSO CO., LTD.) were routinely analyzed alongside nutrient samples (Table S1 in Supporting Information S1). Nanomolar techniques were then employed for those samples whose concentrations were initially identified as being below 0.1 μmol L^{-1} for N + N and 0.08 μmol L^{-1} for PO_4^{3-} via analysis by the AA3 Auto-Analyzer. Nanomolar phosphate samples (typically above 200 m) were collected and immediately determined onboard by using a sequential injection system combined with a HLB solid-phase extraction cartridge (Ma et al., 2008). The standard calibration was performed in the range of 0–80 nmol L^{-1}. The detection limit was 2.1 nmol L^{-1} and the analytical precision was 7.4% (repeat measurements of aged deep seawater with 1,000-fold dilution, 27.5 ± 2.0 nmol L^{-1}, $n = 56$). Nanomolar N + N samples (typically above 200 m) were collected and frozen at −20°C until analysis on land. Measurements were conducted using a continuous flow analysis system (without gas-segmented constitute) combined with a liquid waveguide capillary flow cell (J. Z. Zhang, 2000). The standard calibration was performed in the range of 0–200 nmol L^{-1}. The detection limit was 3.7 nmol L^{-1} (10 × the standard deviation of the blanks) and the analytical precision was 6.4% (repeat measurements of aged deep seawater with 1000-fold dilution, 39.5 ± 2.5 nmol L^{-1}, $n = 56$).

DO samples were collected in 60 mL biological oxygen demand bottles and measured onboard within ∼12 hr using the spectrophotometric Winkler method (Labasque et al., 2004). Before measurement, the samples were placed in a thermostatic bath at 25.00 ± 0.01°C for ∼1 hr. Subsequently, spectrophotometric analysis was performed at 466 nm using the SHIMADZU UV-1800 Spectrophotometer (Shimadzu Suzhou Instruments Manufacturing CO., LTD.). The repeatability of 12 samples taken from the same Niskin sampling bottle was 0.18% at the 200 μmol L^{-1} level. The relative standard deviation of the slopes of standard curves was 0.25% ($n = 11$). The differences between the duplicate samples were <1 μmol L^{-1} ($n = 968$).

Table 1
Comparison of Biogeochemical Parameters Within Four Transects

	E2-1		E2-2		E2-3		E2-4	
Parameter	Core	Edge	Core	Edge	Core	Edge	Core	Edge
Station	E2MM	E2L[a], E2R[a]	A32[a]	A31[a], A34	Z2, A34[a], Z3	Z4[a], Z5[a], Z6, A32, Z7[a]	Z1[a], Z2[a], A34[a]	A36, A35, Z4[a], Z6[a]
SLA (cm)	–7	6 ± 1	–9	2 ± 5	–11 ± 3	–2 ± 6	–8 ± 1	–2 ± 4
MLD (m)	40	36 ± 10	52	34 ± 4	30 ± 6	46 ± 5	17 ± 4	22 ± 8
Nutricline (m)	91	124 ± 28	101	127 ± 14	90 ± 7	107 ± 17	105 ± 12	128 ± 10
DCM depth (m)	103	133 ± 32	125	131 ± 13	97 ± 7	122 ± 12	114 ± 16	130 ± 9
Euphotic zone depth (m)	148	162 ± 15	158	161 ± 6	146 ± 3	157 ± 6	153 ± 8	161 ± 5
N + N (nmol L^{-1}, mean in the MLD)	9.8 ± 0.4	8.7 ± 4.0	5.2 ± 0.9	5.7 ± 1.3	6.3 ± 2.4	10.5 ± 6.0	7.5 ± 0.4	6.5 ± 3.9
PO_4^{3-} (nmol L^{-1}, mean in the MLD)	20.8 ± 3.2	34.6 ± 4.3	16.3 ± 1.0	27.3 ± 3.9	18.3 ± 2.8	24.1 ± 4.7	15.7 ± 2.9	20.7 ± 4.8
Diapycnal N + N flux (μmol m^{-2} d^{-1})[b]	189.5	7.0 ± 4.3	7.8	3.4 ± 0.6	47.0 ± 69.5	18.2 ± 9.8	15.1 ± 12.5	17.5 ± 12.2
Diapycnal PO_4^{3-} flux (μmol m^{-2} d^{-1})[b]	12.3	0.1 ± 0	1.1	0.2 ± 0.1	4.3 ± 6.5	1.4 ± 1.2	1.0 ± 0.7	1.0 ± 0.3
Largest N/P ratio	15.5	15.2 ± 0.1	17.2	15.2 ± 0.1	16.1 ± 1.3	15.3 ± 0.3	18.7 ± 1.9	15.5 ± 0.1
Surface N_2 fixation (nmol N L^{-1} d^{-1})[c]	0.85 ± 0.44	0.18 ± 0.19 and 0.30 ± 0.12	2.39 ± 0	0.87 ± 0.12	2.49 ± 0.26 and 2.34 ± 0.13	0.71 ± 0.04	–	–
POC (mmol C m^{-2}, 0–200 m)	209	256 ± 18	181	175 ± 18	229	198 ± 11	202 ± 24	215 ± 37
PON (mmol N m^{-2}, 0–200 m)	22.6	28.3 ± 4.0	22.3	16.2 ± 1.7	26.6	21.1 ± 1.8	23.9 ± 6.0	23.4 ± 3.9
POC:PON ratio	9.2	9.1 ± 0.7	8.1	10.8 ± 0.1	8.6	9.5 ± 1.4	8.8 ± 2.4	9.2 ± 0.8
TChl *a* (mg m^{-2}, 0–200 m)	3.0	7.0 ± 3.0	23.7	18.4 ± 12.1	15.7 ± 4.8	10.7 ± 4.1	20.9 ± 2.9	20.4 ± 5.1

[a]Indicates the station whose euphotic zone depth was estimated from the equation $Z_{eu} = 0.47 \times DCM + 99.95$. [b]Calculated as the effective diapycnal flux into the euphotic zone. [c]Mean ± standard deviations of triplicate measurements per station.

2.3. N_2 Fixation and Particulate Organic Carbon/Nitrogen (POC/PON)

Rates of N_2 fixation were determined using the enriched water method (Mohr et al., 2010; Wilson et al., 2012). The $^{15}N_2$-enriched seawater was made with $^{15}N_2$ gas (98.9 atom %, Cambridge Isotope Laboratories) according to Shiozaki et al. (2015). In order to determine whether $^{15}N_2$ gas stock contained ^{15}N-labeled ammonium, nitrate and/or nitrite, and nitrous oxide contaminants (see Dabundo et al. (2014)), a blank check for $^{15}N_2$ gas was performed (Lu et al., 2018). The $\delta^{15}N$ values of total dissolved nitrogen (including ammonium, nitrate and/or nitrite, and nitrous oxide) from natural seawater with and without $^{15}N_2$ gas injection were 5.0 and 4.7‰, respectively, suggesting no potential contamination of the stock. Samples for N_2 fixation analyses were collected in triplicate 1.2 L Nalgene polycarbonate bottles at six or seven depths from surface to 180 m (detailed depth profiles of N_2 fixation rates will be presented in another independent manuscript). Samples were spiked with 100 mL $^{15}N_2$-enriched filtered seawater prepared at the same site. The final $^{15}N_2$ enrichment in the incubation bottles was not measured directly during this research cruise. Instead, the dissolved $^{15}N_2$ atom % was measured in a shore-based laboratory by simulating the onboard incubation procedures (same approach, reagents, and equipment as for the field study described here). Measurements were conducted using membrane inlet mass spectrometry, and the $^{15}N_2$ atom % in the incubation bottles ranged from 8.30 to 8.55 atom %, with a mean ± s.d. of 8.42 ± 0.09 atom % ($n = 6$). The average value of 8.42 atom % $^{15}N_2$ enrichment was used to calculate N_2 fixation rates in this study. Samples were placed in on-deck incubators cooled by flowing surface seawater. Incubators were screened with neutral density and blue filters (061 Mist blue; 172 Lagoon Blue), which maintained near in-situ irradiance. During the incubation period, the light intensity was monitored on deck with a flat 2π PAR

sensor (PQS 1 PAR Quantum sensor) at one-minute intervals. After 24 hr of incubation, water samples were filtered onto pre-combusted (450°C, 4 hr) 25 mm glass fiber filters (GF/75, 0.3 μm pore size; Advantec), and the particle samples at the beginning were also collected to determine background $\delta^{15}N$ values. All the filters were immediately frozen onboard at −20°C. The PON on the filters was oxidized to NO_3^- using the wet digestion method (Knapp et al., 2005; Wan et al., 2018). Briefly, each filter was placed into a 12 mL pre-combusted borosilicate glass tube with 0.3 mL of purified persulfate oxidizing reagent (POR) and 5 mL of deionized water (MilliQ, Millipore), tightly capped, and autoclaved for 1 hr under 120°C, after which sample pH was adjusted to neutral with 6 mol L^{-1} HCl (ACS-grade, Merck). The NO_3^- concentration after digestion was measured by the chemiluminescence method (Braman & Hendrix, 1989). Before the use of POR, the residual NO_3^- concentration in the initial POR (referred to as POR blank) was measured and ensured to be less than 2 μmol L^{-1} in the digested solution. In addition, the unused filters were randomly selected to estimate the filter blank (less than 6 nmol N). The POR blank and filter blank typically accounted for less than 1% and 3% of the total N content in our samples, respectively. The $\delta^{15}N$ values of the PON-derived NO_3^- were determined using the denitrification bacterial method coupled to a GasBench isotope ratio mass spectrometer (Thermo Fisher Delta V) in a shore-based laboratory (Casciotti et al., 2002; Sigman et al., 2001). The $\delta^{15}N$ values of NO_3^- were calibrated against NO_3^- isotope standards USGS 34, IAEA N3 and USGS 32, with analytical accuracies better than ±0.3‰ according to analyses of these standards at an injection level of 20 nmol N. The N_2 fixation rates were then calculated according to Montoya et al. (1996). The detection limits were constrained by taking 4‰ as the minimum acceptable change in $\delta^{15}N$ of PON, which corresponded to a range of 0.02–0.08 nmol N L^{-1} d^{-1} for PON concentrations ranging from 0.12 to 0.20 μmol N L^{-1}.

Samples for POC/PON analyses were filtered through pre-combusted 25 mm diameter Whatman QM-A quartz microfiber filters (1.0 μm pore size). Filters were dried overnight onboard at 50°C and stored in polycarbonate dishes for analysis on land. Filters were analyzed after carbonate removal by acid fumigation using a PE-2400 SERIES II CHNS/O elemental analyzer according to the JGOFS protocols (Knap et al., 1996). Acetanilide (Merck) standards were routinely analyzed alongside every set of eight samples. The average blank values for C and N in the filters were 6.4 and 1.4 μg, respectively. The precision was better than 10% based on replicate analyses of random samples.

2.4. Phytoplankton Community Structure

Samples for phytoplankton diagnostic pigment analyses were filtered onto 47 mm diameter Whatman GF/F filters, frozen at −80°C, then later extracted with 2 mL of a N,N-dimethylformamide solution and analyzed using an Agilent series 1100 HPLC system (Huang et al., 2010). Total chlorophyll *a* (TChl *a*) was calculated as the summation of chlorophyll *a* and divinyl chlorophyll *a*. The chemical taxonomy program CHEMTAX was adopted to estimate the contribution of different phytoplankton groups to the TChl *a* concentration (Mackey et al., 1996; Wang et al., 2018). Phytoplankton size groups were classified into picophytoplankton (<2 μm; *Prochlorococcus* + *Synechococcus* + prasinophytes), nanophytoplankton (2–20 μm; haptophyte-6 + haptophyte-8 + chlorophytes + cryptophytes), and microphytoplankton (>20 μm; diatoms + dinoflagellates) (Sieburth et al., 1978; Wang et al., 2018).

2.5. Calculation of Isopycnal Anomalies and Effective Nutrient Diapycnal Fluxes

The isopycnal anomalies of nutrients and DO were calculated to constrain biogeochemical changes triggered by prior physical-biological processes, assuming similar initial concentrations for a given isopycnal surface (Barone et al., 2022). Here station E2L was selected as a reference station as it was least disturbed by Eddy E2 or an adjacent anticyclonic eddy, and the anomalies were derived by the concentrations difference between the stations of interest and station E2L along the same isopycnal, with the following formula:

$$S_{anomaly} = C_t - C_{E2L} \quad (1)$$

where C_t and C_{E2L} are the substance (i.e., N + N, PO_4^{3-}, DO) concentration of targeted station and station E2L at a given density, respectively, and $S_{anomaly}$ is the associated concentration anomaly. $S_{anomaly}$ was then interpolated at a one-m vertical resolution using linear interpolation.

Nutrient consumption is accompanied by concurrent DO accumulation (or vice versa). To assess if the isopycnal anomalies of nutrients and DO were consistent with the stoichiometric ratio of the production or remineralization of organic matter, the excess DO anomaly (Excess $DO_{anomaly}$) was calculated as follows:

$$\text{Excess } DO_{anomaly} = -AOU_{anomaly} + R_{O_2:P} \times PO_4^{3-}{}_{anomaly} \quad (2)$$

where AOU is the apparent oxygen utilization calculated as the difference between the DO concentration in equilibrium with the atmosphere at in situ temperature and salinity and the observed DO concentration, $R_{O_2:P} = 150$ is the modified Redfield ratio of DO production to phosphate uptake (Anderson, 1995), and $PO_4^{3-}{}_{anomaly}$ is the phosphate anomaly. Here we use phosphate anomaly rather than regularly used N + N anomaly (e.g., Abell et al., 2005; Johnson et al., 2010) because concentrations of N + N are ubiquitously depleted to levels around or below the detection limit in the upper nutricline in this system (~10 nmol L^{-1}, the top of the nutricline depth was defined as the 0.1 μmol L^{-1} N + N contour). Ideally, the excess DO anomaly is expected to be close to 0 provided that the water initially had the same isopycnal concentration as station E2L and was subsequently altered according to the modified Redfield ratio ($R_{O_2:P} = 150$), and any deviation from this value suggests a decoupling between DO production (consumption) and nutrient consumption (production), with other potential processes being involved.

The effective diapycnal fluxes (F_{eff}) of N + N and phosphate were calculated following Du et al. (2017) using the field turbulence and nutrient measurements. Briefly, vertical profiles of the turbulence microstructure were measured twice at each station by using a loosely tethered VMP500 profiler (Rockland Scientific International). The profiler was launched from the sea surface to approximately 500 m depth, free-falling at a speed of 0.5–0.7 m s^{-1}. The turbulent kinetic energy dissipation rate (ε) was estimated by fitting the Nasmyth spectrum to the measured shear spectra (Z. Liu et al., 2017). The diapycnal diffusivity (K_V) and velocity (w) were then calculated from in situ estimates of ε and neutral density surface analysis, respectively. The effective diapycnal flux (F_{eff}) to the water column between depth z and the sea surface was calculated as the summation of diapycnal diffusive flux (F_{diff}) and advective flux (F_{adv}) across the isopycnal, and along isopycnal divergence or convergence flux (F_H):

$$F_{eff} = F_{diff} + F_{adv} + F_H = -K_V \frac{\partial c}{\partial z} + wc + \int_z^0 c \frac{\partial w}{\partial z} dz \quad (3)$$

where c is the nutrient concentration at depth z, $\frac{\partial c}{\partial z}$ is the vertical gradient of c, and $\frac{\partial w}{\partial z}$ is the vertical gradient of w. For this calculation, nutrient depth profiles were first interpolated at a 1-m vertical resolution and fluxes were subsequently calculated at each meter. It should be noted that the derived fluxes will be sensitive to both the numbers and the time of the microstructure profiles were made, with the potential for diurnal variability in these measurements.

3. Results

3.1. Dynamic Structure of Eddy E2

Satellite altimetry measurements showed that Eddy E2 had depressed surface heights and counterclockwise surface current circulation, demonstrating a cyclonic eddy (Figures 1b–1f and Figure S1 in Supporting Information S1). The eddy first formed at 133.375°E, 18.375°N around the 10 February 2019, then persisted for 4 months, and ultimately disappeared around the 10 June 2019 in the western boundary of Northwest Pacific (at 123.625°E, 19.125°N; Figures 1a and 1b). Based on a previously proposed age model (Rii et al., 2008; Sweeney et al., 2003), we split the whole lifespan of eddy E2 into three broad stages, with an intensification phase from around 10 February to 20 March, a mature phase from around 20 March to 18 May, and a decay phase from around 18 May to 10 June. Our four repeat-transect observations of Eddy E2 were made within the second month of its appearance (with the center drifting ~193 km in this time period; Figure 1b), we therefore attribute our four visits to a well-developed mature phase. The successive SLA images showed Eddy E2 propagated west during our occupation and our transects nearly intersected its center (Figures 1c–1f). In order to better elucidate spatial differentiation of properties within Eddy E2, we categorized the study stations into eddy core, eddy edge, and outer, which were defined as the stations whose depths of potential density anomaly of 23.5 kg m^{-3} (approaching the upper boundary of the DCM) were (a) shoaled to above 100 m, (b) between 100 and 150 m, and (c) below 150 m, respectively (Table 1). Acknowledging the somewhat arbitrary nature of this definition, it nonetheless allows for a valuable framework for discerning the spatial differences in upwelling intensity. During four visits, the SLA within the eddy core first deepened from −7 to −11 cm (E2-1 to E2-3) and then shoaled to −8 cm (E2-4; Table 1). It was noteworthy that station A35 in transects E2-2 and E2-3, which were classified as outer stations according to the aforementioned definition, were actually located within an anticyclonic eddy paired with our targeted cyclonic Eddy E2, with the SLA of 21 and 19 cm, respectively (Figure S1 in Supporting Information S1). In all cases, vertical depth profiles along the transects showed that shoaling of temperature and salinity isolines were more pronounced within the core of Eddy E2 relative to its edge and outer stations, with lower temperature and higher salinity at equivalent depths (Figures 2a–2h).

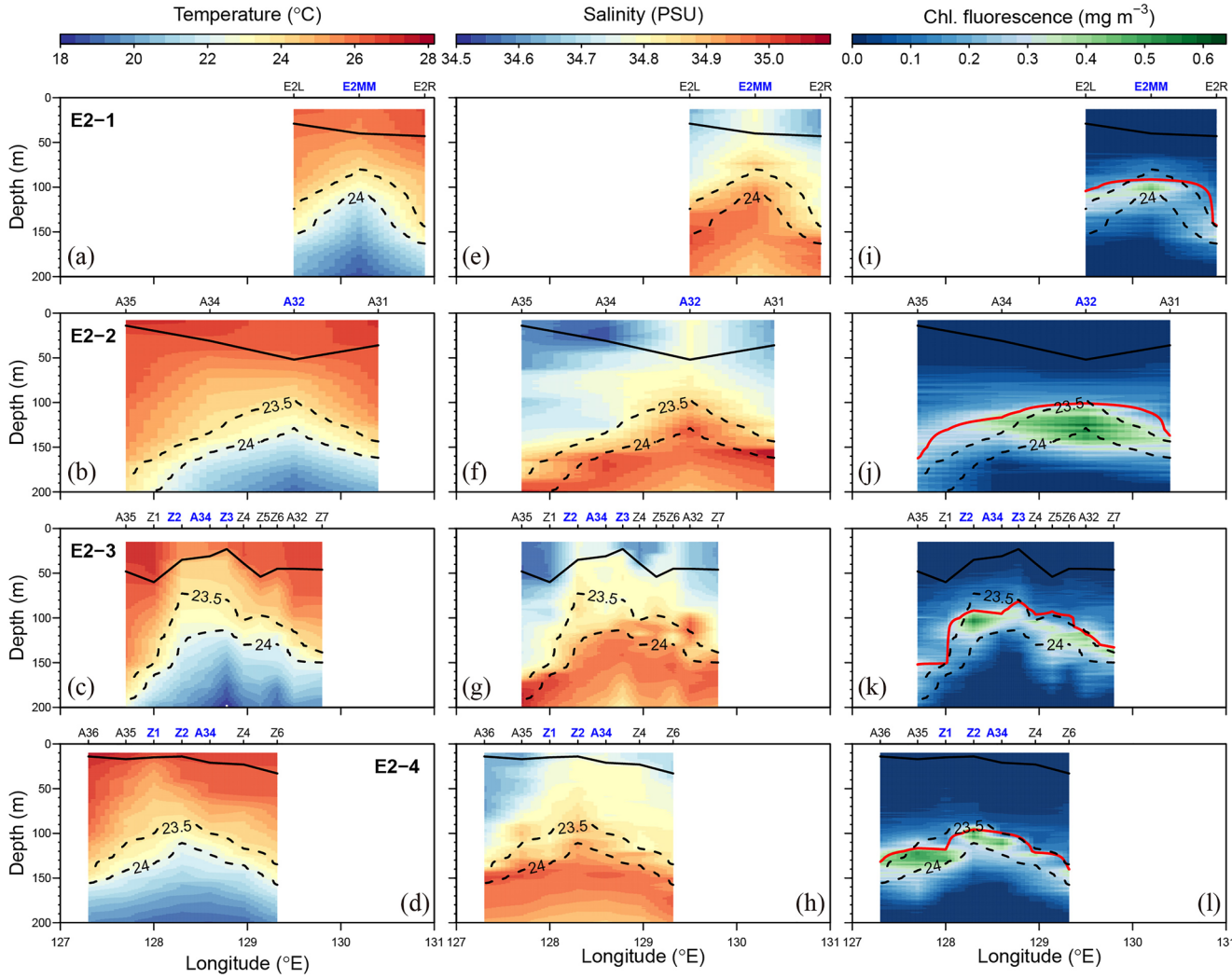

Figure 2. Depth sections of hydrological features and in situ chlorophyll (Chl) fluorescence along the four transects. (a–d) Temperature; (e–h) Salinity; and (i–l) Chl fluorescence. Black solid lines denote the depth of the base of the mixed layer. Black dashed lines denote the depth of isopycnal surfaces with potential density anomaly of 23.5 and 24 kg m^{-3} (approximately situated within the upper and lower boundaries of the deep Chl maximum). Red solid lines in the right panel denote the depth of the top of the nutricline. Labels on the top of each panel represent the position of the sampling stations, with blue labels highlighting the core stations.

3.2. Nutrient and DO Responses to Eddy E2

Amongst our four visits, the concentrations of N + N were consistently very low in the mixed layer both within the core and at the edge of Eddy E2 (on average 7.9 ± 4.2 nmol L^{-1}; Figure S2 in Supporting Information S1; Table 1). Larger differences were however observed below the nutricline, with higher concentrations within the core than at the edge (Figures 3a–3d). In contrast to N + N, phosphate concentrations showed distinct spatial differences in the mixed layer, with coherently lower concentrations within the Eddy E2 core relative to the edge (Figures 3e–3h; Table 1). This spatial pattern was further extended to the waters above the nutricline (e.g., on average 18.2 ± 3.9 nmol L^{-1} at station A32 of the Eddy E2-2 core, n = 9; on average 28.3 ± 4.4 nmol L^{-1} at station A31 of the Eddy E2-2 edge, n = 14; Figure 4a–4c). The lower phosphate concentrations at depths shallower than the nutricline were matched by corresponding higher signals in DO, with higher concentrations of DO occurring within the Eddy E2 core compared to those at the edge (Figures 3i–3l and 4d–4f). For example, the differences in DO concentration between the E2-3 core and edge above the nutricline were as large as 7.7 μmol L^{-1} at the same depth (Figure 4e). Unlike N + N or phosphate, the uplift of silicate within the eddy core across all observations exhibited an outcropped, elevated silicate isosurface (Figures 3m–3p), consistent with the observed distribution of salinity (Figures 2e–2h). Further density plots confirmed exactly the same results; specifically, lower phosphate and higher DO in the Eddy E2 core than the edge along the same isopycnal above

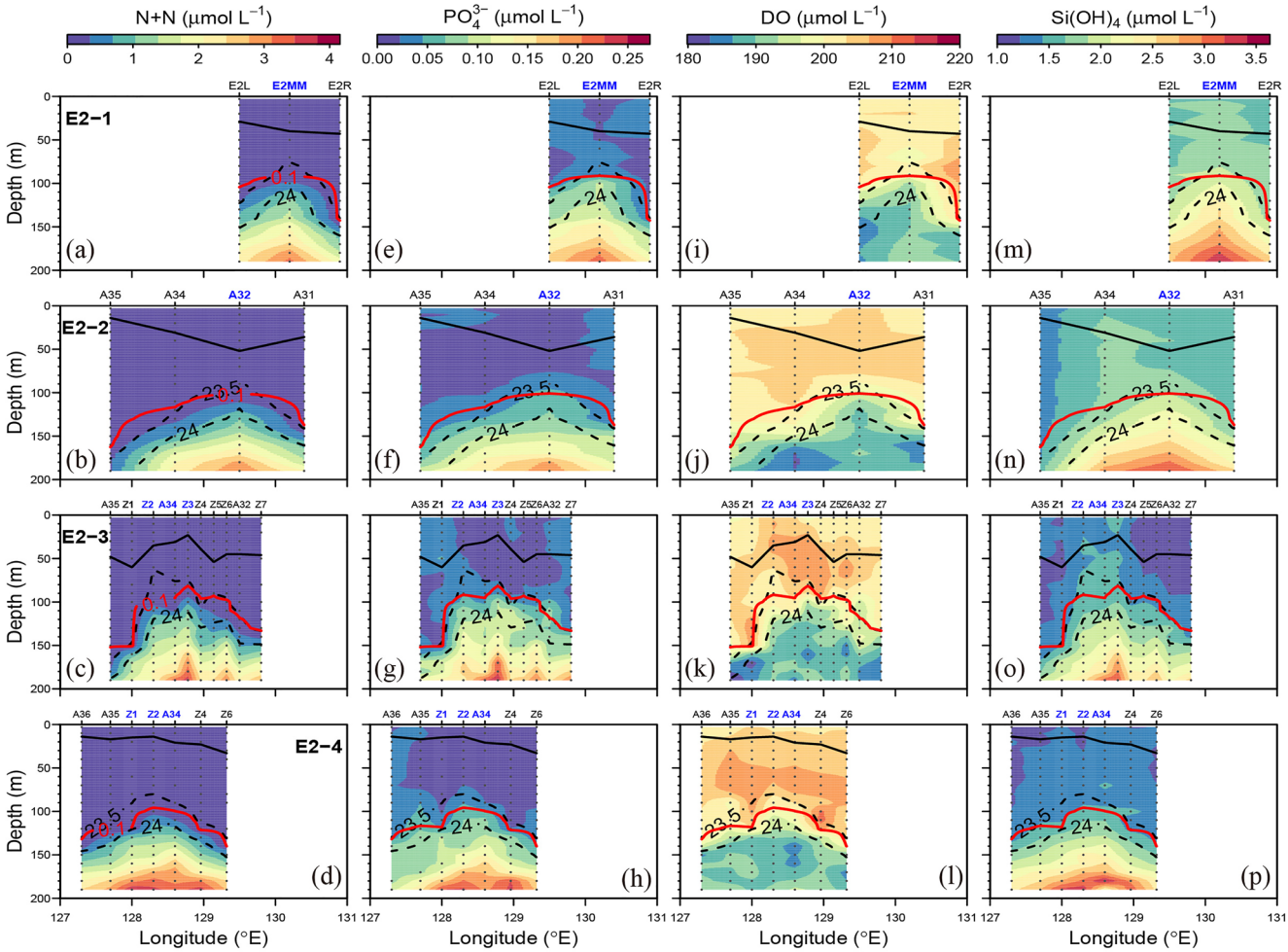

Figure 3. Depth sections of nutrients and Dissolved oxygen along the four transects. (a–d) N + N; (e–h) PO_4^{3-}; (i–l) DO; and (m–p) $Si(OH)_4$. Black dots represent the sampling points. Black solid lines denote the depth of the base of the mixed layer. Black dashed lines denote the depth of isopycnal surfaces with potential density anomaly of 23.5 and 24 kg m^{-3} (approximately situated within the upper and lower boundaries of the deep Chl maximum). Red solid lines denote the depth of the top of the nutricline. Labels on the top of each panel represent the position of the sampling stations, with blue labels highlighting the core stations.

the nutricline contour (Figures S3 and S4 in Supporting Information S1). In line with the relatively narrow range of SLA within the core (−7 to −11 cm), the temporal evolution of Eddy E2 had comparable impacts on nutrient distribution. Specifically, the nutricline depths within the core, which could be equivalent to nutrient injection intensity, exhibited no significant differences across our four sequential observations (Table 1).

We also observed noticeable anomalies of both N + N and DO along the isopycnal surfaces situated at the depths surrounding the band of DCM layer, with the larger negative N + N anomalies corresponding to the larger positive DO anomalies within the core (Figures 5a–5d and 5i–5l). The patterns of phosphate anomalies were similar but less robust than that of N + N, with negative signals occasionally penetrating all the way to the surface (Figures 5e–5h). Moreover, the excess DO anomalies were gradually elevated following the four sequential observations around the band of DCM layer, from the maximum of 5.9 to 16.2 μmol L^{-1}, whereas these excess DO anomalies were consistently negative below the DCM layer, suggesting that the stoichiometry of nutrients and DO deviated from that predicted for production and consumption of phytoplankton biomass (Figures 5m–5p).

When compiling all four transects together, we noticed distinct variations across the stations (Figures 6a and 6b). Specifically, the SLA exhibited a range of 13–21 cm, indicating significant spatiotemporal variability (Figure 6a). This variability in SLA was closely related to the vertical displacement of the nutricline depths, which ranged from 82 to 163 m (Figure 6b). Clearly, we found that the most negative SLA corresponded to the shallowest nutricline depth at the core stations, whereas the most positive SLA aligned with the deepest nutricline depth

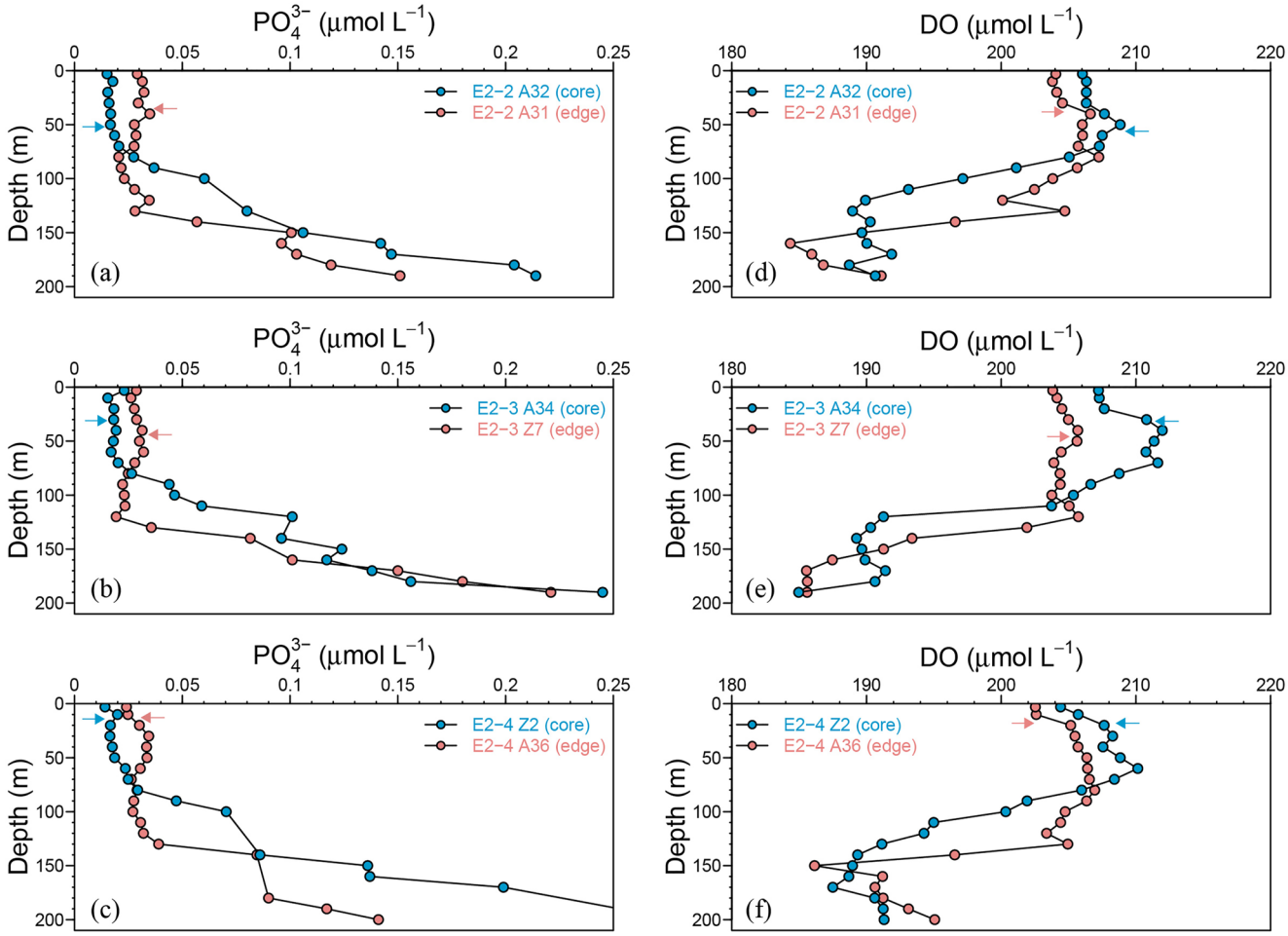

Figure 4. Representative depth profiles of PO_4^{3-} and Dissolved oxygen (DO) concentrations for the core (blue) and edge (pink) stations in Eddy E2-2, E2-3, and E2-4. (a–c) PO_4^{3-} and (d–f) DO. Arrows denote the depth of the base of the mixed layer.

at the anticyclonic stations (station A35 in transects E2-2 and E2-3; Figures 6a and 6b). By integrating nutrient concentration over the upper 60 m, a depth which was uniformly shallower than the observed nutricline depths at all stations (82–163 m), we found that the integrated N + N concentrations were generally low without any distinct trend between the core, edge, and anticyclonic stations (Figure 6b; Table 1; Figure S5 in Supporting Information S1); in contrast, the integrated phosphate concentrations were much clearer, with ∼1.2–1.6-fold lower inventories at core stations compared to those present at edge and anticyclonic stations (Figure 6b; Table 1).

Upward displacement of the nutricline associated with the core of eddy E2 resulted in enhanced nutrient diapycnal fluxes into the euphotic zone, except for transect E2-4, where no significant differences could be observed (Table 1). For example, the vertical N + N and phosphate diapycnal fluxes into the euphotic zone were calculated to be 2.3-fold and 5.5-fold higher within the core of Eddy E2-2 relative to its edge, respectively (Table 1). The highest diapycnal fluxes of N + N and phosphate into the euphotic zone were observed at the core of Eddy E2-1, which was primarily attributed to the shallower nutricline depth, resulting in a more substantial vertical gradient at the depth of euphotic zone (Table 1).

3.3. Biological Responses to Eddy E2

Spatial and temporal variability in the physical structure of Eddy E2 appeared to result in a biological response. The vertical position of DCM, confined within a narrow band of isopycnal surfaces with σ_t of 23.5 and 24 kg m^{-3}, also varied synchronously with the vertical displacement of water masses (Figures 2i–2l). For example, the DCM depth in Eddy E2-3 shoaled from 122 m at the edge to 97 m within the core (Table 1).

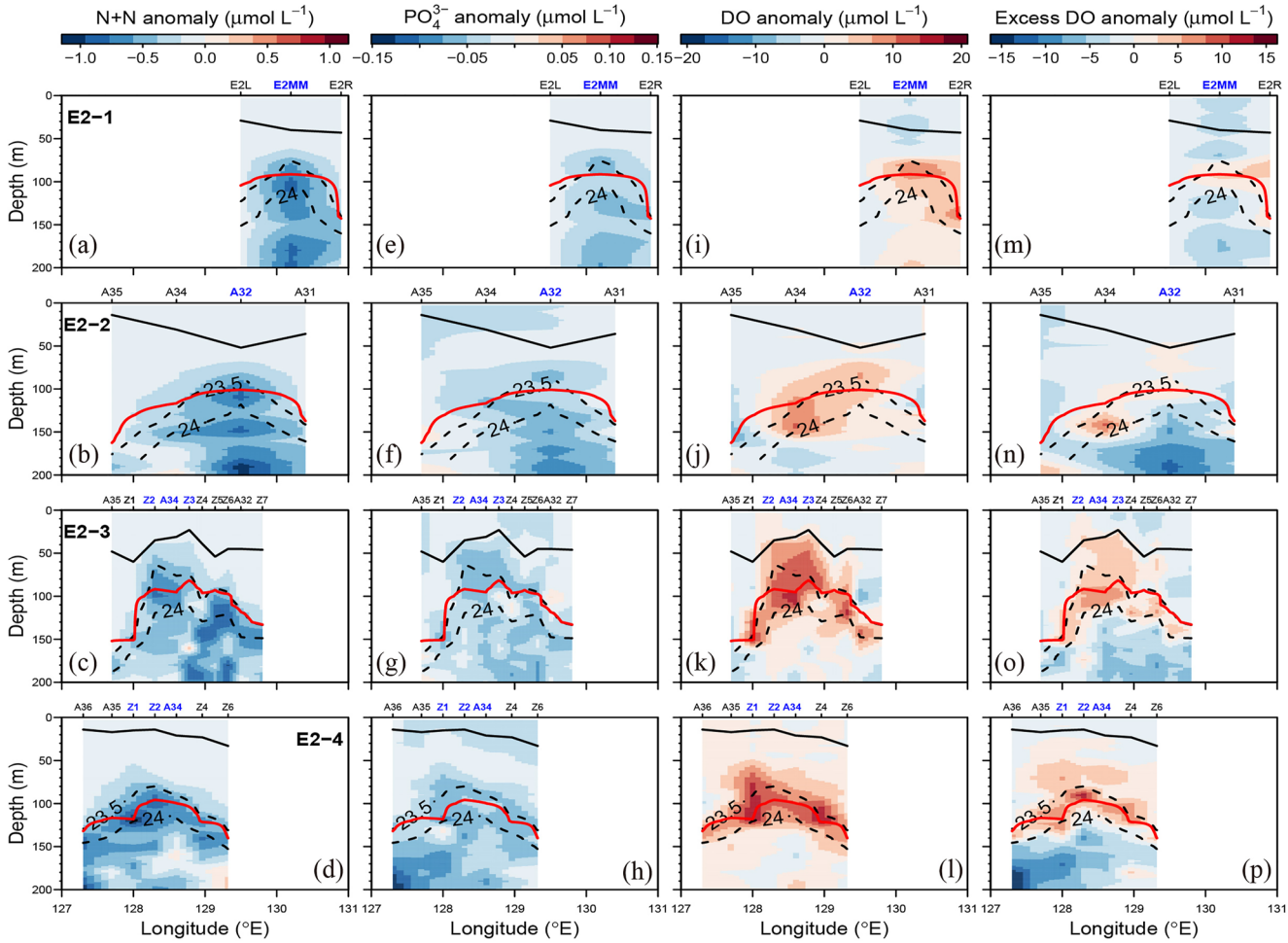

Figure 5. Depth sections of nutrient and Dissolved oxygen (DO) anomalies along the four transects. (a–d) N + N anomaly; (e–h) PO_4^{3-} anomaly; (i–l) DO anomaly; (m–p) Excess DO anomaly. Black solid lines denote the depth of the base of the mixed layer. Black dashed lines denote the depth of isopycnal surfaces with potential density anomaly of 23.5 and 24 kg m^{-3} (approximately situated within the upper and lower boundaries of the deep Chl maximum). Red solid lines denote the depth of the top of the nutricline. Labels on the top of each panel represent the position of the sampling stations, with blue labels highlighting the core stations.

Moreover, more intense chlorophyll fluorescence was observed within the core rather than at the edge (Figures 2i–2l). This spatial pattern, however, was not reflected in the TChl *a* inventories above 200 m, with no clear trends across the stations (Figure 6d; Table 1). In terms of the phytoplankton community, picophytoplankton consistently dominated the phytoplankton assemblage, contributing to >70% of TChl *a* inventories. In contrast, microphytoplankton accounted for less than 2% of TChl *a* inventories (Figure 6d). Despite their low proportions, microphytoplankton exhibited clear spatial variations, with generally higher microphytoplankton Chl *a* inventories observed at the core stations of transects E2-2, E2-3, and E2-4 (Figure 6d). The inventories of fucoxanthin, a biomarker pigment of diatoms (Uitz et al., 2006), also exhibited 1.6-fold, 1.6-fold, and 1.1-fold increases at the core stations of transects E2-2, E2-3, and E2-4, respectively (data not shown). The POC and PON inventories in the upper 200 m exhibited no discernible trends across the stations. However, the ratios of POC:PON varied, with lower values observed within the eddy core, although these differences were not always statistically significant, when compared to the eddy edge at transects E2-2, E2-3, and E2-4 (Figure 6c; Table 1).

Surface N_2 fixation rates measured on the first three transects were around 3-fold greater within the Eddy E2 core than at the edge (Figure 6a; Table 1). Although our number of N_2 fixation observations was limited, the inverse relationship between N_2 fixation and SLA was significant ($R^2 = 0.73$, $n = 7$, $p = 0.014$; Figure 7a).

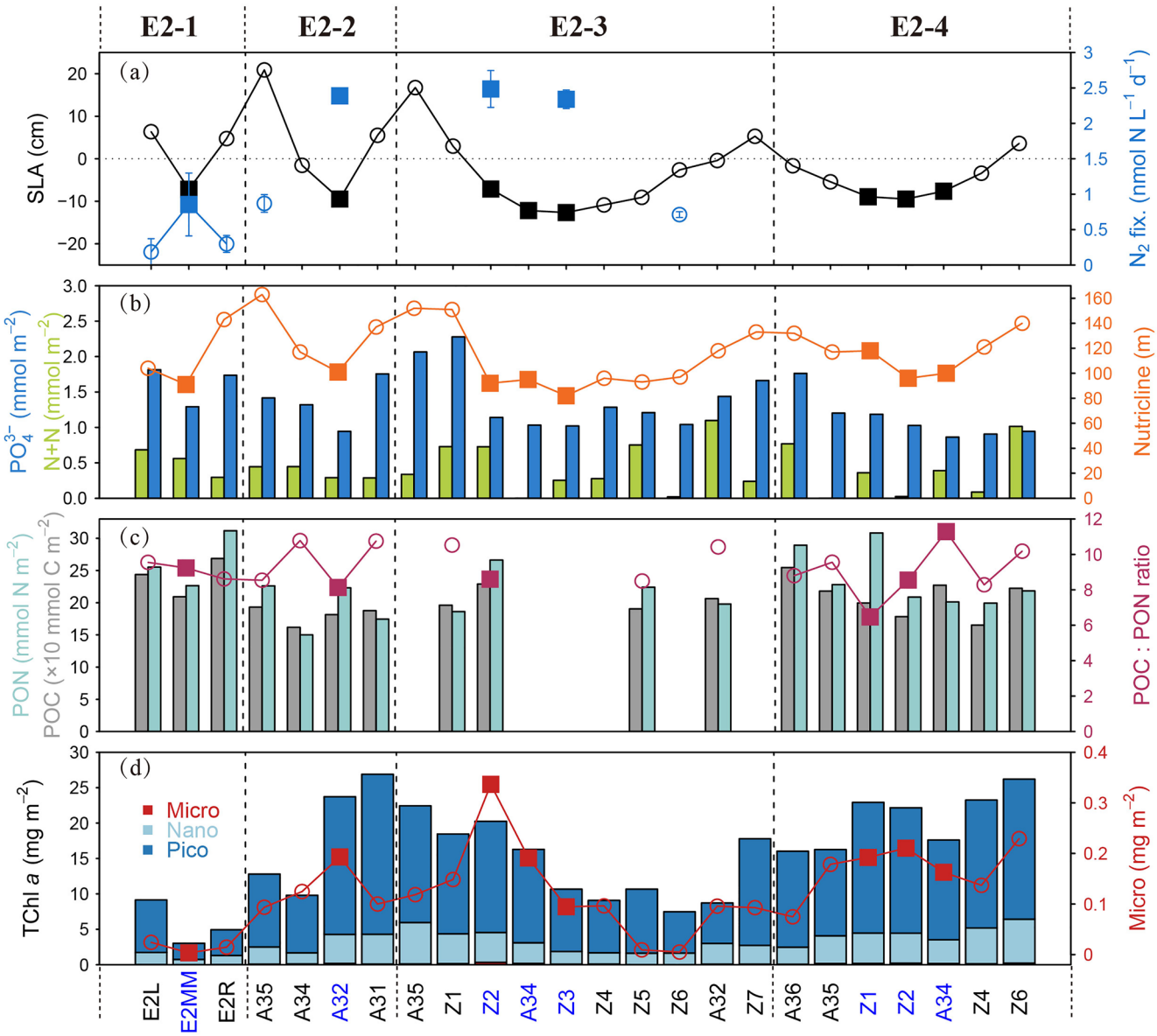

Figure 6. Biogeochemical features at each station during the cruise. (a) Surface distribution of sea level anomaly and N_2 fixation rate. Error bars represent the standard deviations of triplicate measurements; (b) N + N and PO_4^{3-} inventories in the upper 60 m overplotted with nutricline depth; (c) POC and PON inventories in the upper 200 m overplotted with POC:PON ratio; (d) Grouped TChl *a* inventory in the upper 200 m overplotted with microphytoplankton Chl *a* inventory. Note that the proportion of microphytoplankton Chl *a* inventory is consistently too low to be visually discernible in the stacked bar chart. Stations labeled in blue and the filled squares represent the core stations of Eddy E2.

4. Discussion

4.1. Mechanisms Controlling Phosphate Drawdown

To our best knowledge, we found the first observations of significantly lower phosphate concentrations above the nutricline within the core relative to the edge of a subtropical cyclonic eddy, including a significant positive correlation between the mean phosphate concentration in the mixed layer and the corresponding SLA ($R^2 = 0.45$, $n = 24$, $p = 3.0 \times 10^{-4}$; Figure 7b). This is in contrast with the expectation of higher nutrient concentrations within the eddy core, driven by elevated nutrient supply due to the shoaled nutriclines (e.g., Barone et al., 2022; Benitez-Nelson et al., 2007; Falkowski et al., 1991; Hawco et al., 2021; McGillicuddy et al., 1998, 2007; Zhou et al., 2023). What regulated this? We hypothesize a mechanism whereby enhanced phosphate drawdown within the eddy core relative to the edge is driven by elevated phosphate consumption via stimulated N_2 fixation.

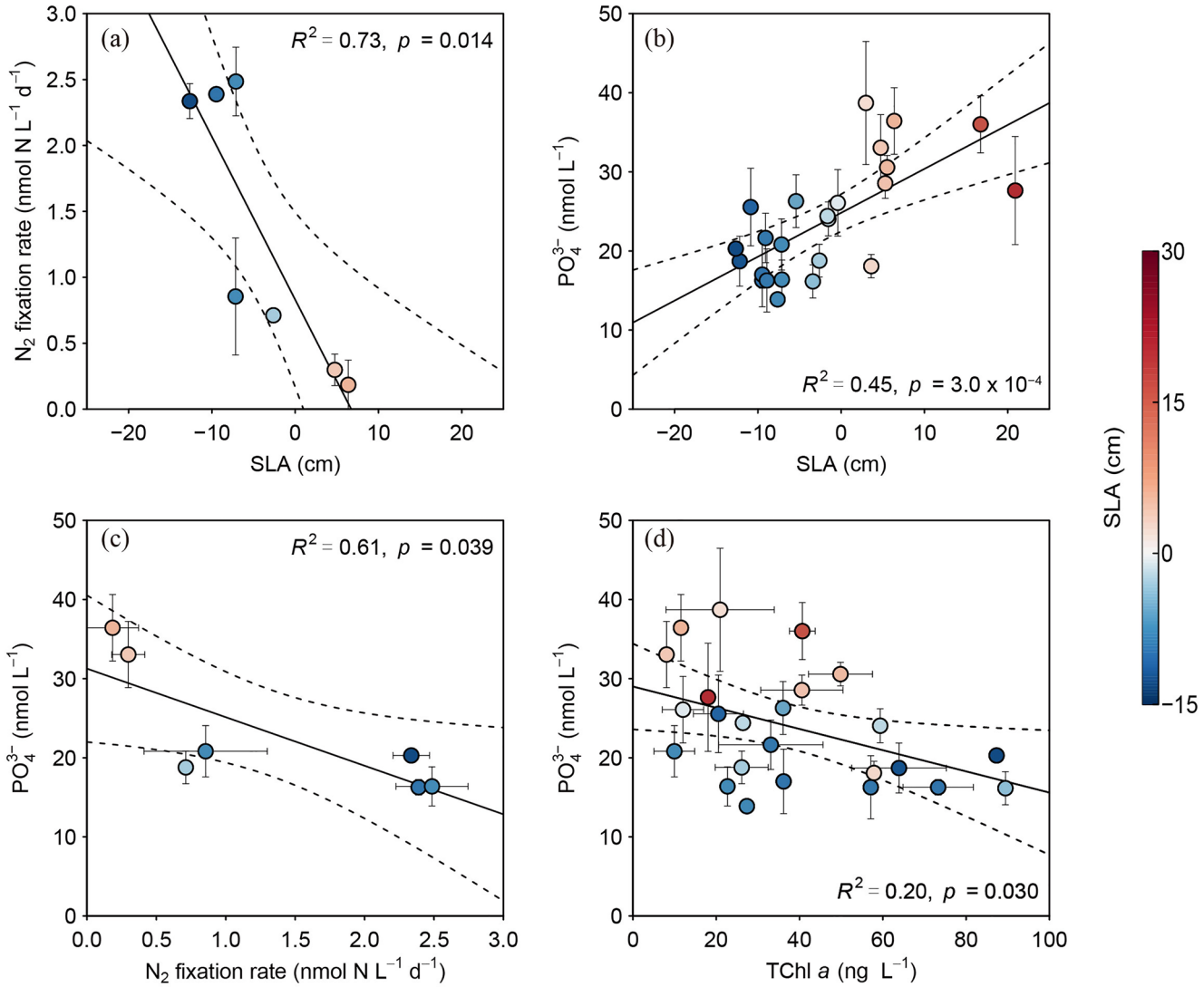

Figure 7. Correlations among the mean concentrations of PO_4^{3-} and TChl *a* in the mixed layer, surface N_2 fixation rate, and sea level anomaly (SLA) (a–d). The dashed lines indicate the 95% confidence band. Colored circles represent SLA.

Specifically, the negative correlation of mean phosphate concentration in the mixed layer with surface N_2 fixation rate suggested that N_2 fixation plays a significant role in regulating the residual standing phosphate concentration ($R^2 = 0.61$, $n = 7$, $p = 0.039$; Figure 7c). We further found that mean phosphate and TChl *a* concentrations in the mixed layer showed a significant, but less strong relationship ($R^2 = 0.20$, $n = 24$, $p = 0.030$; Figure 7d), indicating bulk phytoplankton uptake might have a minor effect in driving phosphate drawdown. More broadly, when extending to deeper depths above the nutricline, such as 30, 60, and 80 m, we observed a consistent relationship between depth-integrated phosphate and TChl *a* inventories, surface N_2 fixation rate, and SLA, although the relationship becomes less clear at the integration depth of 80 m compared to 30 and 60 m, which could be associated with its closer proximity to the nutricline allowing for more phosphate to penetrate into this layer from deeper nutrient-enriched depths (Figure S6 in Supporting Information S1).

A footprint of our eddy-enhanced N_2 fixation hypothesis is furthermore potentially reflected in the enhanced N + N to phosphate (N/P) ratios within the core of Eddy E2 relative to its edge, via the remineralization of newly fixed N + N below the euphotic zone (Figure 8 and Figure S7 in Supporting Information S1). Specifically, our results showed that in the lower euphotic zone, the largest N/P ratios at the eddy core stations were higher than those at the edge stations (Table 1). Some of these higher N/P ratios at the core stations of transects E2-2, E2-3, and E2-4 approached, or even exceeded the Redfield N/P ratio of 16 (Redfield et al., 1963). These values were

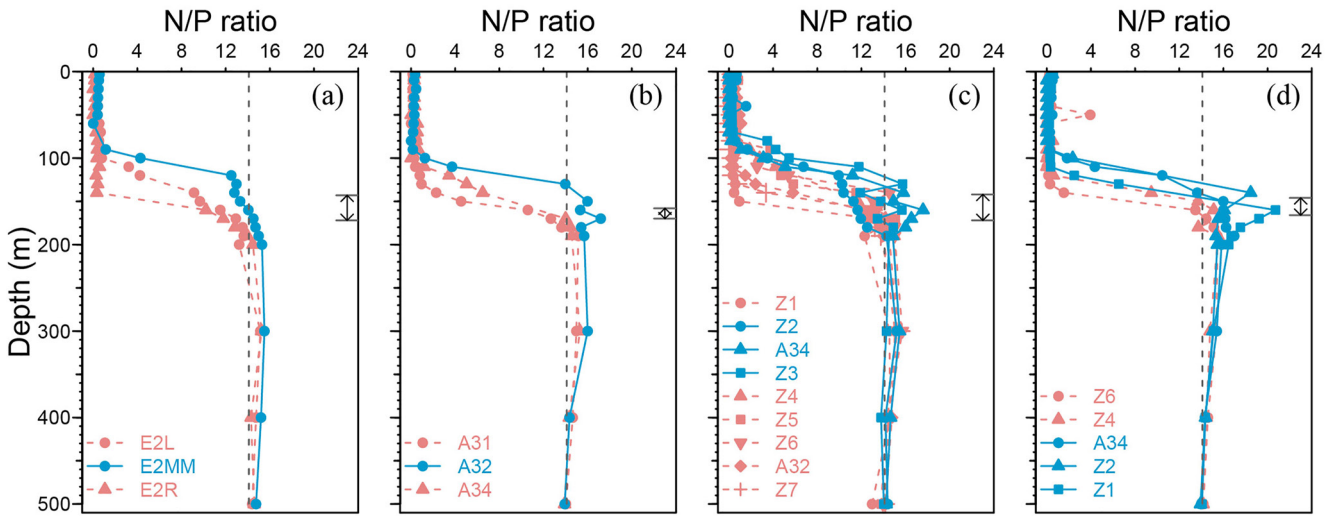

Figure 8. Depth profiles of N + N to PO_4^{3-} (N/P) ratios for the four transects. (a) E2-1; (b) E2-2; (c) E2-3; and (d) E2-4. Only the stations that remained continuously within Eddy E2 were included. Therefore, station A35 and station A36, which were previously located in an anticyclonic eddy (see Figure 1d), were excluded from the data set. Blue and pink colored profiles represent the core and edge stations, respectively. Vertical dashed line represents the mean N/P ratio of 14.1 at 500 m over all stations (n = 24). The arrow denotes the range of the base of the euphotic zone (0.1% light level) at each transect.

therefore far beyond the interior thermocline N/P ratio (14.1 ± 0.3, n = 24; derived from mean value at 500 m over all stations), suggesting that the observed N/P ratios of >16 at the core stations cannot be explained by the uplift of deeper thermocline waters. Moreover, denitrification in the below thermocline oxygen-deficient waters could lead to even lower N/P ratios due to the removal of N + N to N_2. Instead, provided that atmospheric deposition, typically characterized by an N/P ratio of >500 (Baker et al., 2010; Martino et al., 2014), remained uniform over the short timescale of our study, we propose that the observed higher N/P ratios of >16 below the euphotic zone at the eddy core stations were likely a result of the intense remineralization of organic matter derived from N_2-fixing diazotrophs from overlying waters, which have a higher N/P ratio of >16 (White et al., 2006; Zehr & Capone, 2020).

It has been found that mesoscale eddies induced by instabilities in large-scale currents can isolate water parcels for several months whilst transporting the trapped properties for hundreds of kilometers from their origin (Chelton, Gaube, et al., 2011; Early et al., 2011; Gaube et al., 2014; Lehahn et al., 2011). Across our four transects, the eventual transect E2-4 shows a relative relaxation in uplifted isopycnal surfaces; subduction of these waters would therefore transport this N-enriched organic matter downwards from surface layers, together with gravitational sinking of these particles, which would be efficiently mineralized below the euphotic zone and lead to a significant increase in ambient N/P ratios (i.e., >16; Figure 8; Benitez-Nelson et al., 2007; noting that the horizontal advection of water masses from the core to the edge could partially contribute to affecting the spatial differences). Over longer timescales, entrainment of these thermocline waters with elevated N/P ratios into surface waters would contribute to broader scale P deficiency in the region (Browning et al., 2022; Hashihama et al., 2009, 2021; Kitajima et al., 2009; Martiny et al., 2019; Shiozaki et al., 2010; Wen et al., 2022; Yuan et al., 2023).

The observation of cyclonic eddy-induced enhanced N_2 fixation is unexpected with the general perception that increases in diazotrophy occur instead within anticyclonic eddies, where N supply is reduced (Böttjer et al., 2017; Cheung et al., 2020; Church et al., 2009; Davis & McGillicuddy, 2006; Dugenne et al., 2023; Fong et al., 2008; Holl et al., 2007; J. Liu et al., 2020; Löscher et al., 2016; Wilson et al., 2017). Indeed, reduced N supply rates might be expected to favor diazotrophs by increasing their competitiveness with non-diazotrophic phytoplankton that grow faster when N is available (Landolfi et al., 2015; Wu et al., 2000). However, with other factors remaining the same, diazotrophy is likely strongly dependent on the relative supply rates of both N and Fe, due to elevated Fe requirements for nitrogenase enzyme activity (Berman-Frank et al., 2001; Ward et al., 2013). Therefore, provided the uplift of deeper, nutrient-enriched waters in Eddy E2 supplied sufficient Fe relative to N, enhanced N_2 fixation might be expected. Wen et al. (2022) estimated that Fe:N supply rates to the euphotic zone in this

region was 3.4×10^{-4} (surface Fe ~0.2 nmol L^{-1}), which was approximately one order of magnitude higher than the assumed-average, non-diazotrophic phytoplankton requirements of 4.7×10^{-5} (Moore, 2016). This high Fe:N supply rate is expected to cause available N to be fully depleted before Fe, by fueling non-diazotrophic phytoplankton growth in the DCM layer after upward transport through eddy injection (Figures 3a–3d; McGillicuddy & Robinson, 1997). Consumption of P at 1/16 of N would lead to a relative excess of available phosphate, as N/P of waters below the euphotic zone of background waters is <16 (Figure 8). Given Fe limitation of the growth of N_2-fixing diazotrophs in this region (Wen et al., 2022), any residual Fe entrained into waters above the DCM should thus favor the growth of N_2-fixing diazotrophs within upper waters of the cyclonic eddy, in turn leading to the observed drawdown of excess phosphate. Apart from the proposed Fe-stimulated N_2 fixation within the core of the cyclonic eddy, it appears unlikely that bottom-up control factors, such as light and temperature, played a significant role. Surface light conditions were expected to be similar between the core and the edge, indicating that light availability alone cannot explain the observed increase in N_2 fixation. Furthermore, the relatively lower surface temperature within the core may have even resulted in decreased N_2 fixation rates, which is opposite to what was observed (Luo et al., 2014). Similarly, the expected increase in zooplankton grazing of phytoplankton within the eddy core could potentially reduce, rather than increase, the abundance of diazotrophs (Dugenne et al., 2023; Wilson et al., 2017). Additionally, it has been suggested that the physical accumulation of diazotrophs primarily takes place in regions characterized by strong frontal downwelling, rather than within the core of a cyclonic eddy where upwelling is prominent (Dugenne et al., 2023).

We thus conclude that cyclonic eddy-induced enhanced N_2 fixation within the eddy core was primarily due to the excess surface phosphate, alongside the likely elevated iron supply from depth. Indeed, the linkage between elevated iron supply–enhanced N_2 fixation–phosphate drawdown has been well-established (Mahaffey et al., 2005; Sohm et al., 2011; Zehr & Capone, 2021). Numerous studies have explored the role of iron supply in promoting N_2 fixation in different oceanic regions. For example, iron supply from atmospheric deposition has been hypothesized to favor N_2 fixation in the North Atlantic (Moore et al., 2009; Wu et al., 2000) and North Pacific (Browning et al., 2022; Hashihama et al., 2009; Kitajima et al., 2009; Wen et al., 2022; Yuan et al., 2023). Additionally, the iron supply from the ocean interior has also been identified as a potential driving mechanism for a hotspot for N_2 fixation in the nitrate-depleted Angola Gyre of the South Atlantic (Marshall et al., 2022) and western tropical South Pacific (Bonnet et al., 2017, 2023).

4.2. Biogeochemical Responses to Eddy E2

We found the most prominent anomalies of both N + N and DO occurred surrounding the DCM layer (Figure 5), suggesting that the uplift of nutrient-enriched waters into the DCM layer enabled significant biological uptake of nutrients and production of DO. Thus, the DCM layer served as a buffer zone limiting the impact of eddies extending to the near-surface ocean (Barone et al., 2022). Moreover, our results also identified that the cyclonic eddy could decouple changes in nutrients and DO concentrations. Over our relatively short duration for each transect, provided limited ventilation of DO occurred below the mixed layer, additional biological processes must be involved. So far, several mechanisms have been proposed to address these positive excess DO anomalies around the band of DCM layer and negative excess DO anomalies down below, including (a) production of carbon-enriched dissolved organic matter (Abell et al., 2005; Fawcett et al., 2018), (b) formation of transparent exopolymer particles (TEPs, Letscher & Villareal, 2018), (c) the vertical migration of phytoplankton (Barone et al., 2022; Letscher & Villareal, 2018), and (d) consumption of N + N by heterotrophic bacteria (Fawcett et al., 2018; Letscher & Villareal, 2018). Although we cannot evaluate the relative contribution of these mechanisms that may have likely led to the observed excess DO anomalies, accumulation of external new nitrogen from enhanced N_2 fixation would likely be another option (Fawcett et al., 2018). This process can result in more DO production and thus leads to the increasing positive excess DO anomalies with eddy evolution. In this case, the subsequent decomposition of these N-enriched organic matter could partly explain the negative excess DO anomalies below the DCM layer. We thus suggest the enhanced N_2 fixation in the surface should play a vital role in the observed excess DO anomalies. This was further supported by the not significantly but lower POC:PON values observed at the eddy core stations of transects E2-2, E2-3, and E2-4 (Figure 6c; Table 1).

We also observed more intense chlorophyll fluorescence around the DCM within the eddy core. We suggest this was likely due to the combined effects of the enhanced upward nutrient supply and increased light availability. Cyclonic eddy uplift of deeper waters resulted in the shoaling of the nutricline, thereby leading to

increased diapycnal nutrient fluxes delivered to the lower euphotic zone (Table 1). Moreover, this uplift also displaced the light-limited DCM community to a shallower depth with higher light intensities (Figures 2i–2l). Consequently, the combination of nutrient enrichment and improved light conditions within the eddy core created an environment conducive to more enhanced phytoplankton growth and biomass accumulation. Nevertheless, we did not observe any substantial enhancement in TChl *a* over the entire euphotic zone, which was probably due to concomitant increases in grazing rates. This was further supported by the persistent dominance of picophytoplankton (>70%) in these waters, whose growth is expected to be tightly coupled to losses by zooplankton grazing (Calbet & Landry, 2004; McAndrew et al., 2007). In addition, despite slight enhancements in microphytoplankton biomass (also fucoxanthin, the biomarker of diatoms) at the core stations of Eddy E2-2, E2-3, and E2-4, the core of Eddy E2 was notably not dominated by microphytoplankton, with their contribution to TChl *a* inventories only accounting for less than 2% (Figure 6d). This was consistent with a previous study conducted near this region where the authors hypothesized this to be a result of the low nutrient supply into the euphotic zone as well as the chemical composition of nutrients (Yun et al., 2020). In contrast, the well-developed cyclonic eddy *Opal* off the Hawaiian Islands displayed a large diatom bloom that accounted for ∼80% of the total carbon-based biomass, which was 100-fold higher than background levels (Benitez-Nelson et al., 2007; Brown et al., 2008). It is difficult to attribute this difference between these eddies to any particular mechanism, with differences in upwelling intensity, the duration of uplift of nutrient-enriched isopycnals, and sampling timing potentially all playing important roles (Rii et al., 2008). In fact, remote sensing showed that Eddy E2 evolved with further depressed sea surface height until it reached a minimum SLA a month after our observations (Figure 1b). Hence, it is reasonable to presume that Eddy E2 has the potential of forming a diatom bloom provided upward nutrient supply are intense enough and of long enough duration.

5. Conclusions

Our observations demonstrated enhanced phosphate consumption above the nutricline within the core of a subtropical cyclonic eddy in the Northwest Pacific, which was likely due to elevated N_2 fixation driven by enhanced Fe supply relative to N. This region is characterized by primary N limitation of the bulk phytoplankton community (Browning et al., 2022; Yuan et al., 2023), indicating that phosphate is presently sufficiently available for supporting phytoplankton growth. However, climate forcing has been proposed to be enhancing eddy activity in this region (Matear et al., 2015), which could contribute to the further drawdown of residual phosphate in surface waters, and potentially eventually drive this system to a situation where phytoplankton become P stressed (Martin et al., 2014; Van Mooy et al., 2009). Further detailed assessments of eddies on nutrient biogeochemistry such as that presented here, in conjunction with the resolution of dissolved Fe, will be crucial for better elucidating how an altered frequency of these episodic events will impact the broader oceanic biogeochemistry of this region in the future.

Data Availability Statement

Biogeochemical data collected onboard used in this study are available on the Science Data Bank (Yuan & Dai, 2023, https://doi.org/10.57760/sciencedb.08040). The altimetric Mesoscale Eddy Trajectories Atlas (META3.1exp DT) was distributed by AVISO+ (Pegliasco et al., 2021, https://doi.org/10.24400/527896/A01-2021.001). Daily sea level anomaly (SLA) at 0.25° resolution was obtained from the Copernicus Climate Change Service Climate Data Store (2018) (https://doi.org/10.24381/cds.4c328c78). The satellite-derived chlorophyll *a* for April 2019 at 9 km resolution was downloaded from the NASA Ocean Biology Processing Group (2019) (https://oceancolor.gsfc.nasa.gov/l3/order/).

Acknowledgments
We thank three anonymous reviewers and the Editor for their constructive comments. We thank the captain and other crew of R/V TKK for their cooperation during the cruise. Tao Huang, Lifang Wang, Liguo Guo, Weifang Chen, and Wen Lin are thanked for their assistance in sample analysis. Haoran Liu is thanked for his helpful discussion. Yanping Xu and Zhe Wang are thanked for their logistical assistance. This study was supported by the National Natural Science Foundation of China (Grants 41890804 and 41730533). Z. Yuan was supported by the Chinese Scholarship Council (File 202106310003).

References

Abell, J., Emerson, S., & Keil, R. G. (2005). Using preformed nitrate to infer decadal changes in DOM remineralization in the subtropical North Pacific. *Global Biogeochemical Cycles*, *19*(1), 1–16. https://doi.org/10.1029/2004GB002285

Allen, C. B., Kandat, J., & Laws, E. A. (1996). New production and photosynthetic rates within and outside a cyclonic mesoscale eddy in the North Pacific subtropical gyre. *Deep-Sea Research I*, *43*(6), 917–936. https://doi.org/10.1016/0967-0637(96)00022-2

Anderson, L. A. (1995). On the hydrogen and oxygen content of marine phytoplankton. *Deep-Sea Research I*, *42*(9), 1675–1680. https://doi.org/10.1016/0967-0637(95)00072-E

Baker, A. R., Lesworth, T., Adams, C., Jickells, T. D., & Ganzeveld, L. (2010). Estimation of atmospheric nutrient inputs to the Atlantic Ocean from 50°N to 50°S based on large-scale field sampling: Fixed nitrogen and dry deposition of phosphorus. *Global Biogeochemical Cycles*, *24*(3), GB3006. https://doi.org/10.1029/2009GB003634

Barone, B., Church, M. J., Dugenne, M., Hawco, N. J., Jahn, O., White, A. E., et al. (2022). Biogeochemical dynamics in adjacent mesoscale eddies of opposite polarity. *Global Biogeochemical Cycles*, *36*(2), e2021GB007115. https://doi.org/10.1029/2021GB007115

Benitez-Nelson, C. R., Bidigare, R. R., Dickey, T. D., Landry, M. R., Leonard, C. L., Brown, S. L., et al. (2007). Mesoscale Eddies drive increased silica export in the subtropical Pacific Ocean. *Science*, *316*(5827), 1017–1021. https://doi.org/10.1126/SCIENCE.1136221

Berman-Frank, I., Cullen, J. T., Shaked, Y., Sherrell, R. M., & Falkowski, P. G. (2001). Iron availability, cellular iron quotas, and nitrogen fixation in Trichodesmium. *Limnology and Oceanography*, *46*(6), 1249–1260. https://doi.org/10.4319/lo.2001.46.6.1249

Bonnet, S., Caffin, M., Berthelot, H., & Moutin, T. (2017). Hot spot of N_2 fixation in the western tropical South Pacific pleads for a spatial decoupling between N_2 fixation and denitrification. *Proceedings of the National Academy of Sciences of the United States of America*, *114*(14), E2800–E2801. https://doi.org/10.1073/pnas.1619514114

Bonnet, S., Guieu, C., Taillandier, V., Boulart, C., Bouruet-Aubertot, P., Gazeau, F., et al. (2023). Natural iron fertilization by shallow hydrothermal sources fuels diazotroph blooms in the ocean. *Science*, *380*(6647), 812–817. https://doi.org/10.1126/science.abq4654

Böttjer, D., Dore, J. E., Karl, D. M., Letelier, R. M., Mahaffey, C., Wilson, S. T., et al. (2017). Temporal variability of nitrogen fixation and particulate nitrogen export at Station ALOHA. *Limnology and Oceanography*, *62*(1), 200–216. https://doi.org/10.1002/lno.10386

Braman, R. S., & Hendrix, S. A. (1989). Nanogram nitrite and nitrate determination in environmental and biological materials by vanadium(III) reduction with chemiluminescence detection. *Analytical Chemistry*, *61*(24), 2715–2718. https://doi.org/10.1021/ac00199a007

Brown, S. L., Landry, M. R., Selph, K. E., Jin Yang, E., Rii, Y. M., & Bidigare, R. R. (2008). Diatoms in the desert: Plankton community response to a mesoscale eddy in the subtropical North Pacific. *Deep-Sea Research II*, *55*(10–13), 1321–1333. https://doi.org/10.1016/j.dsr2.2008.02.012

Browning, T. J., Al-Hashem, A. A., Hopwood, M. J., Engel, A., Belkin, I. M., Wakefield, E. D., et al. (2021). Iron regulation of North Atlantic Eddy phytoplankton productivity. *Geophysical Research Letters*, *48*(6), e2020GL091403. https://doi.org/10.1029/2020GL091403

Browning, T. J., Liu, X., Zhang, R., Wen, Z., Liu, J., Zhou, Y., et al. (2022). Nutrient co-limitation in the subtropical Northwest Pacific. *Limnology And Oceanography Letters*, *7*(1), 52–61. https://doi.org/10.1002/lol2.10205

Calbet, A., & Landry, M. R. (2004). Phytoplankton growth, microzooplankton grazing, and carbon cycling in marine systems. *Limnology and Oceanography*, *49*(1), 51–57. https://doi.org/10.4319/lo.2004.49.1.0051

Casciotti, K. L., Sigman, D. M., Hastings, M. G., Böhlke, J. K., & Hilkert, A. (2002). Measurement of the oxygen isotopic composition of nitrate in seawater and freshwater using the denitrifier method. *Analytical Chemistry*, *74*(19), 4905–4912. https://doi.org/10.1021/ac020113w

Chaigneau, A., Eldin, G., & Dewitte, B. (2009). Eddy activity in the four major upwelling systems from satellite altimetry (1992-2007). *Progress in Oceanography*, *83*(1–4), 117–123. https://doi.org/10.1016/J.POCEAN.2009.07.012

Chelton, D. B., Gaube, P., Schlax, M. G., Early, J. J., & Samelson, R. M. (2011). The influence of nonlinear mesoscale eddies on near-surface oceanic chlorophyll. *Science*, *334*(6054), 328–332. https://doi.org/10.1126/science.1208897

Chelton, D. B., Schlax, M. G., & Samelson, R. M. (2011). Global observations of nonlinear mesoscale eddies. *Progress in Oceanography*, *91*(2), 167–216. https://doi.org/10.1016/j.pocean.2011.01.002

Cheung, S., Nitanai, R., Tsurumoto, C., Endo, H., Nakaoka, S. I., Cheah, W., et al. (2020). Physical forcing controls the basin-scale occurrence of nitrogen-fixing organisms in the North Pacific Ocean. *Global Biogeochemical Cycles*, *34*(9), e2019GB006452. https://doi.org/10.1029/2019GB006452

Church, M. J., Mahaffey, C., Letelier, R. M., Lukas, R., Zehr, J. P., & Karl, D. M. (2009). Physical forcing of nitrogen fixation and diazotroph community structure in the North Pacific subtropical gyre. *Global Biogeochemical Cycles*, *23*(2), GB2020. https://doi.org/10.1029/2008GB003418

Copernicus Climate Change Service Climate Data Store. (2018). Sea level gridded data from satellite observations for the global ocean from 1993 to present [Dataset]. Copernicus Climate Change Service (C3S) Climate Data Store (CDS). https://doi.org/10.24381/cds.4c328c78

Dabundo, R., Lehmann, M. F., Treibergs, L., Tobias, C. R., Altabet, M. A., Moisander, P. H., & Granger, J. (2014). The contamination of commercial $^{15}N_2$ gas stocks with ^{15}N-labeled nitrate and ammonium and consequences for nitrogen fixation measurements. *PLoS One*, *9*(10), e110335. https://doi.org/10.1371/journal.pone.0110335

Dai, M., Luo, Y.-W., Achterberg, E. P., Browning, T. J., Cai, Y., Cao, Z., et al. (2023). Upper ocean biogeochemistry of the oligotrophic North Pacific Subtropical Gyre: From nutrient sources to carbon export. *Reviews of Geophysics*, *61*(3), e2022RG000800. https://doi.org/10.1029/2022RG000800

Davis, C. S., & McGillicuddy, D. J. (2006). Transatlantic abundance of the N_2-fixing colonial cyanobacterium Trichodesmium. *Science*, *312*(5779), 1517–1520. https://doi.org/10.1126/SCIENCE.1123570

De Boyer Montégut, C., Madec, G., Fischer, A. S., Lazar, A., & Iudicone, D. (2004). Mixed layer depth over the global ocean: An examination of profile data and a profile-based climatology. *Journal of Geophysical Research*, *109*(12), 1–20. https://doi.org/10.1029/2004JC002378

Du, C., Liu, Z., Kao, S., & Dai, M. (2017). Diapycnal fluxes of nutrients in an oligotrophic oceanic regime: The South China Sea. *Geophysical Research Letters*, *44*(22), 11510–11518. https://doi.org/10.1002/2017GL074921

Duce, R. A., LaRoche, J., Altieri, K., Arrigo, K. R., Baker, A. R., Capone, D. G., et al. (2008). Impacts of atmospheric anthropogenic nitrogen on the open ocean. *Science*, *320*(5878), 893–897. https://doi.org/10.1126/science.1150369

Ducklow, H. W., Steinberg, D. K., & Buesseler, K. O. (2001). Upper ocean carbon export and the biological pump. *Oceanography*, *14*(4), 50–58. https://doi.org/10.5670/oceanog.2001.06

Dufois, F., Hardman-Mountford, N. J., Greenwood, J., Richardson, A. J., Feng, M., & Matear, R. J. (2016). Anticyclonic eddies are more productive than cyclonic eddies in subtropical gyres because of winter mixing. *Science Advances*, *2*(5), 1–7. https://doi.org/10.1126/sciadv.1600282

Dugenne, M., Gradoville, M. R., Church, M. J., Wilson, S. T., Sheyn, U., Harke, M. J., et al. (2023). Nitrogen fixation in mesoscale eddies of the North Pacific Subtropical gyre: Patterns and mechanisms. *Global Biogeochemical Cycles*, *37*(4), e2022GB007386. https://doi.org/10.1029/2022GB007386

Early, J. J., Samelson, R. M., & Chelton, D. B. (2011). The evolution and propagation of quasigeostrophic ocean eddies. *Journal of Physical Oceanography*, *41*(8), 1535–1555. https://doi.org/10.1175/2011JPO4601.1

Falkowski, P. G., Ziemann, D., Kolber, Z., & Bienfang, P. K. (1991). Role of eddy pumping in enhancing primary production in the ocean. *Nature*, *352*(6330), 55–58. https://doi.org/10.1038/352055a0

Fawcett, S. E., Johnson, K. S., Riser, S. C., Van Oostende, N., & Sigman, D. M. (2018). Low-nutrient organic matter in the Sargasso Sea thermocline: A hypothesis for its role, identity, and carbon cycle implications. *Marine Chemistry*, *207*, 108–123. https://doi.org/10.1016/j.marchem.2018.10.008

Fong, A. A., Karl, D. M., Lukas, R., Letelier, R. M., Zehr, J. P., & Church, M. J. (2008). Nitrogen fixation in an anticyclonic eddy in the oligotrophic North Pac. *ISME Journal*, *2*(6), 663–676. https://doi.org/10.1038/ismej.2008.22

Garçon, V. C., Oschlies, A., Doney, S. C., McGillicuddy, D., & Waniek, J. (2001). The role of mesoscale variability on plankton dynamics in the North Atlantic. *Deep-Sea Research II*, *48*(10), 2199–2226. https://doi.org/10.1016/S0967-0645(00)00183-1

Gaube, P., McGillicuddy, D. J., Chelton, D. B., Behrenfeld, M. J., & Strutton, P. G. (2014). Regional variations in the influence of mesoscale eddies on near-surface chlorophyll. *Journal of Geophysical Research: Oceans*, *119*(12), 8195–8220. https://doi.org/10.1002/2014JC010111

Guidi, L., Calil, P. H. R., Duhamel, S., Björkman, K. M., Doney, S. C., Jackson, G. A., et al. (2012). Does eddy-eddy interaction control surface phytoplankton distribution and carbon export in the North Pacific Subtropical Gyre? *Journal of Geophysical Research*, *117*(2), 1–12. https://doi.org/10.1029/2012JG001984

Han, A., Dai, M., Kao, S. J., Gan, J., Li, Q., Wang, L., et al. (2012). Nutrient dynamics and biological consumption in a large continental shelf system under the influence of both a river plume and coastal upwelling. *Limnology and Oceanography*, *57*(2), 486–502. https://doi.org/10.4319/lo.2012.57.2.0486

Hashihama, F., Furuya, K., Kitajima, S., Takeda, S., Takemura, T., & Kanda, J. (2009). Macro-scale exhaustion of surface phosphate by dinitrogen fixation in the western North Pacific. *Geophysical Research Letters*, *36*(3), L03610. https://doi.org/10.1029/2008GL036866

Hashihama, F., Yasuda, I., Kumabe, A., Sato, M., Sasaoka, H., Iida, Y., et al. (2021). Nanomolar phosphate supply and its recycling drive net community production in the subtropical North Pacific. *Nature Communications*, *12*(1), 1–8. https://doi.org/10.1038/s41467-021-23837-y

Hawco, N. J., Barone, B., Church, M. J., Babcock-Adams, L., Repeta, D. J., Wear, E. K., et al. (2021). Iron depletion in the deep chlorophyll maximum: Mesoscale eddies as natural iron fertilization experiments. *Global Biogeochemical Cycles*, *35*(12), 1–18. https://doi.org/10.1029/2021GB007112

Holl, C. M., Waite, A. M., Pesant, S., Thompson, P. A., & Montoya, J. P. (2007). Unicellular diazotrophy as a source of nitrogen to Leeuwin Current coastal eddies. *Deep-Sea Research II*, *54*(8–10), 1045–1054. https://doi.org/10.1016/J.DSR2.2007.02.002

Huang, B., Hu, J., Xu, H., Cao, Z., & Wang, D. (2010). Phytoplankton community at warm eddies in the northern South China Sea in winter 2003/2004. *Deep-Sea Research II*, *57*(19–20), 1792–1798. https://doi.org/10.1016/J.DSR2.2010.04.005

Johnson, K. S., Riser, S. C., & Karl, D. M. (2010). Nitrate supply from deep to near-surface waters of the North Pacific subtropical gyre. *Nature*, *465*(7301), 1062–1065. https://doi.org/10.1038/nature09170

Karl, D., Letelier, R., Tupas, L., Dore, J., Christian, J., & Hebel, D. (1997). The role of nitrogen fixation in biogeochemical cycling in the subtropical North Pacific Ocean. *Nature*, *388*(6642), 533–538. https://doi.org/10.1038/41474

Kitajima, S., Furuya, K., Hashihama, F., Takeda, S., & Kanda, J. (2009). Latitudinal distribution of diazotrophs and their nitrogen fixation in the tropical and subtropical western North Pacific. *Limnology and Oceanography*, *54*(2), 537–547. https://doi.org/10.4319/LO.2009.54.2.0537

Klein, P., & Lapeyre, G. (2009). The oceanic vertical pump induced by mesoscale and submesoscale turbulence. *Annual Review of Marine Science*, *1*, 351–375. https://doi.org/10.1146/annurev.marine.010908.163704

Knap, A. H., Michaels, A., Close, A. R., Ducklow, H., & Dickson, A. G. (1996). Protocols for the joint global ocean flux study (JGOFS) core measurements. In *JGOFS, reprint of the IOC manuals and guides No. 29* (Vol. 1994, p. 19). UNESCO.

Knapp, A. N., Sigman, D. M., & Lipschultz, F. (2005). N isotopic composition of dissolved organic nitrogen and nitrate at the Bermuda Atlantic Time-series study site. *Global Biogeochemical Cycles*, *19*(1), 1–15. https://doi.org/10.1029/2004GB002320

Labasque, T., Chaumery, C., Aminot, A., & Kergoat, G. (2004). Spectrophotometric winkler determination of dissolved oxygen: Re-examination of critical factors and reliability. *Marine Chemistry*, *88*(1–2), 53–60. https://doi.org/10.1016/j.marchem.2004.03.004

Landolfi, A., Koeve, W., Dietze, H., Kähler, P., & Oschlies, A. (2015). A new perspective on environmental controls of marine nitrogen fixation. *Geophysical Research Letters*, *42*(11), 4482–4489. https://doi.org/10.1002/2015GL063756

Lehahn, Y., D'Ovidio, F., Lévy, M., Amitai, Y., & Heifetz, E. (2011). Long range transport of a quasi isolated chlorophyll patch by an Agulhas ring. *Geophysical Research Letters*, *38*(16), L16610. https://doi.org/10.1029/2011GL048588

Letscher, R. T., Primeau, F., & Moore, J. K. (2016). Nutrient budgets in the subtropical ocean gyres dominated by lateral transport. *Nature Geoscience*, *9*(11), 815–819. https://doi.org/10.1038/ngeo2812

Letscher, R. T., & Villareal, T. A. (2018). Evaluation of the seasonal formation of subsurface negative preformed nitrate anomalies in the subtropical North Pacific and North Atlantic. *Biogeosciences*, *15*(21), 6461–6480. https://doi.org/10.5194/bg-15-6461-2018

Lewis, M. R., Harrison, W. G., Oakey, N. S., Hebert, D., & Platt, T. (1986). Vertical nitrate fluxes in the oligotrophic ocean. *Science*, *234*(4778), 870–873. https://doi.org/10.1126/science.234.4778.870

Li, Q., Legendre, L., & Jiao, N. (2015). Phytoplankton responses to nitrogen and iron limitation in the tropical and subtropical Pacific Ocean. *Journal of Plankton Research*, *37*(2), 306–319. https://doi.org/10.1093/plankt/fbv008

Li, Q. P., & Hansell, D. A. (2008). Nutrient distributions in baroclinic eddies of the oligotrophic North Atlantic and inferred impacts on biology. *Deep-Sea Research II*, *55*(10–13), 1291–1299. https://doi.org/10.1016/j.dsr2.2008.01.009

Liu, J., Zhou, L., Li, J., Lin, Y., Ke, Z., Zhao, C., et al. (2020). Effect of mesoscale eddies on diazotroph community structure and nitrogen fixation rates in the South China Sea. *Regional Studies in Marine Science*, *35*, 101106. https://doi.org/10.1016/j.rsma.2020.101106

Liu, Y., Dong, C., Guan, Y., Chen, D., McWilliams, J., & Nencioli, F. (2012). Eddy analysis in the subtropical zonal band of the North Pacific Ocean. *Deep-Sea Research I*, *68*, 54–67. https://doi.org/10.1016/j.dsr.2012.06.001

Liu, Z., Lian, Q., Zhang, F., Wang, L., Li, M., Bai, X., et al. (2017). Weak thermocline mixing in the North Pacific low-latitude western boundary current system. *Geophysical Research Letters*, *44*(20), 10530–10539. https://doi.org/10.1002/2017GL075210

Löscher, C. R., Bourbonnais, A., Dekaezemacker, J., Charoenpong, C. N., Altabet, M. A., Bange, H. W., et al. (2016). N_2 fixation in eddies of the eastern tropical South Pacific Ocean. *Biogeosciences*, *13*(10), 2889–2899. https://doi.org/10.5194/BG-13-2889-2016

Lu, Y., Wen, Z., Shi, D., Chen, M., Zhang, Y., Bonnet, S., et al. (2018). Effect of light on N_2 fixation and net nitrogen release of Trichodesmium in a field study. *Biogeosciences*, *15*(1), 1–12. https://doi.org/10.5194/BG-15-1-2018

Luo, Y. W., Lima, I. D., Karl, D. M., Deutsch, C. A., & Doney, S. C. (2014). Data-based assessment of environmental controls on global marine nitrogen fixation. *Biogeosciences*, *11*(3), 691–708. https://doi.org/10.5194/bg-11-691-2014

Ma, J., Yuan, D., & Liang, Y. (2008). Sequential injection analysis of nanomolar soluble reactive phosphorus in seawater with HLB solid phase extraction. *Marine Chemistry*, *111*(3–4), 151–159. https://doi.org/10.1016/j.marchem.2008.04.011

Mackey, M. D., Mackey, D. J., Higgins, H. W., & Wright, S. W. (1996). CHEMTAX - A program for estimating class abundances from chemical markers: Application to HPLC measurements of phytoplankton. *Marine Ecology Progress Series*, *144*(1–3), 265–283. https://doi.org/10.3354/MEPS144265

Mahaffey, C., Michaels, A. F., & Capone, D. G. (2005). The conundrum of marine N_2 fixation. *American Journal of Science*, *305*(6–8), 546–595. https://doi.org/10.2475/ajs.305.6-8.546

Marshall, T., Granger, J., Casciotti, K. L., Dähnke, K., Emeis, K. C., Marconi, D., et al. (2022). The Angola Gyre is a hotspot of dinitrogen fixation in the South Atlantic Ocean. *Communications Earth and Environment*, *3*(1), 1–10. https://doi.org/10.1038/s43247-022-00474-x

Martin, P., Dyhrman, S. T., Lomas, M. W., Poulton, N. J., & Van Mooy, B. A. S. (2014). Accumulation and enhanced cycling of polyphosphate by Sargasso Sea plankton in response to low phosphorus. *Proceedings of the National Academy of Sciences of the United States of America*, *111*(22), 8089–8094. https://doi.org/10.1073/pnas.1321719111

Martino, M., Hamilton, D., Baker, A. R., Jickells, T. D., Bromley, T., Nojiri, Y., et al. (2014). Western Pacific atmospheric nutrient deposition fluxes, their impact on surface ocean productivity. *Global Biogeochemical Cycles*, *28*(7), 712–728. https://doi.org/10.1002/2013GB004794

Martiny, A. C., Lomas, M. W., Fu, W., Boyd, P. W., Chen, Y. L., Cutter, G. A., et al. (2019). Biogeochemical controls of surface ocean phosphate. *Science Advances*, *5*(8), 341–369. https://doi.org/10.1126/sciadv.aax0341

Matear, R. J., Chamberlain, M. A., Sun, C., & Feng, M. (2015). Climate change projection for the western tropical Pacific Ocean using a high-resolution ocean model: Implications for tuna fisheries. *Deep-Sea Research II*, *113*, 22–46. https://doi.org/10.1016/J.DSR2.2014.07.003

McAndrew, P. M., Björkman, K. M., Church, M. J., Morris, P. J., Jachowski, N., Williams, P. J. L. B., & Karl, D. M. (2007). Metabolic response of oligotrophic plankton communities to deep water nutrient enrichment. *Marine Ecology Progress Series*, *332*(C), 63–75. https://doi.org/10.3354/meps332063

McGillicuddy, D. J., Anderson, L. A., Bates, N. R., Bibby, T., Buesseler, K. O., Carlson, C. A., et al. (2007). Eddy/Wind interactions stimulate extraordinary mid-ocean plankton blooms. *Science*, *316*(5827), 1021–1026. https://doi.org/10.1126/SCIENCE.1136256

McGillicuddy, D. J., & Robinson, A. R. (1997). Eddy-induced nutrient supply and new production in the Sargasso Sea. *Deep-Sea Research I*, *44*(8), 1427–1450. https://doi.org/10.1016/S0967-0637(97)00024-1

McGillicuddy, D. J., Robinson, A. R., Siegel, D. A., Jannasch, H. W., Johnson, R., Dickey, T. D., et al. (1998). Influence of mesoscale eddies on new production in the Sargasso Sea. *Nature*, *394*(6690), 263–266. https://doi.org/10.1038/28367

Mohr, W., Großkopf, T., Wallace, D. W. R., & LaRoche, J. (2010). Methodological underestimation of oceanic nitrogen fixation rates. *PLoS One*, *5*(9), e12583. https://doi.org/10.1371/JOURNAL.PONE.0012583

Montoya, J. P., Voss, M., Kahler, P., & Capone, D. G. (1996). A simple, high-precision, high-sensitivity tracer assay for N_2 fixation. *Applied and Environmental Microbiology*, *62*(3), 986–993. https://doi.org/10.1128/aem.62.3.986-993.1996

Moore, C. M. (2016). Diagnosing oceanic nutrient defciency. *Philosophical Transactions of the Royal Society A: Mathematical, Physical & Engineering Sciences*, *374*(2081), 20150290. https://doi.org/10.1098/rsta.2015.0290

Moore, C. M., Mills, M. M., Achterberg, E. P., Geider, R. J., Laroche, J., Lucas, M. I., et al. (2009). Large-scale distribution of Atlantic nitrogen fixation controlled by iron availability. *Nature Geoscience*, *2*(12), 867–871. https://doi.org/10.1038/ngeo667

Moore, C. M., Mills, M. M., Arrigo, K. R., Berman-Frank, I., Bopp, L., Boyd, P. W., et al. (2013). Processes and patterns of oceanic nutrient limitation. *Nature Geoscience*, *6*(9), 701–710. https://doi.org/10.1038/ngeo1765

NASA Ocean Biology Processing Group. (2019). Moderate-resolution imaging spectroradiometer (MODIS) Aqua L3 chlorophyll data 2019 reprocessing [Dataset]. OB.DAAC. Retrieved from https://oceancolor.gsfc.nasa.gov/l3/order/

Oschlies, A., & Garçon, V. (1998). Eddy-influenced enhancement of primary production in a model of the North Atlantic Ocean. *Nature*, *394*(6690), 266–269. https://doi.org/10.1038/28373

Pegliasco, C., Delepoulle, A., & Faugère, Y. (2021). Mesoscale eddy trajectories atlas delayed-time all satellites: Version META3.1exp DT allsat (3.1exp DT allsat) [Dataset]. AVISO+. https://doi.org/10.24400/527896/A01-2021.001

Qiu, B., & Chen, S. (2010). Interannual variability of the North Pacific Subtropical Countercurrent and its associated mesoscale eddy field. *Journal of Physical Oceanography*, *40*(1), 213–225. https://doi.org/10.1175/2009JPO4285.1

Redfield, A. C., Ketchum, B. H., & Richards, F. A. (1963). The influence of organisms on the composition of seawater. *The Sea*, *2*, 26–77.

Rii, Y. M., Brown, S. L., Nencioli, F., Kuwahara, V., Dickey, T., Karl, D. M., & Bidigare, R. R. (2008). The transient oasis: Nutrient-phytoplankton dynamics and particle export in Hawaiian lee cyclones. *Deep-Sea Research II*, *55*(10–13), 1275–1290. https://doi.org/10.1016/j.dsr2.2008.01.013

Seki, M. P., Polovina, J. J., Brainard, R. E., Bidigare, R. R., Leonard, C. L., & Foley, D. G. (2001). Biological enhancement at cyclonic eddies tracked with GOES thermal imagery in Hawaiian waters. *Geophysical Research Letters*, *28*(8), 1583–1586. https://doi.org/10.1029/2000GL012439

Shiozaki, T., Furuya, K., Kodama, T., Kitajima, S., Takeda, S., Takemura, T., & Kanda, J. (2010). New estimation of N_2 fixation in the western and central Pacific Ocean and its marginal seas. *Global Biogeochemical Cycles*, *24*(1), GB1015. https://doi.org/10.1029/2009GB003620

Shiozaki, T., Nagata, T., Ijichi, M., & Furuya, K. (2015). Seasonal dynamics of nitrogen fixation and the diazotroph community in the temperate coastal region of the northwestern North Pacific. *Biogeosciences*, *12*, 865–889. https://doi.org/10.5194/bgd-12-865-2015

Sieburth, J. M., Smetacek, V., & Lenz, J. (1978). Pelagic ecosystem structure: Heterotrophic compartments of the plankton and their relationship to plankton size fractions 1. *Limnology and Oceanography*, *23*(6), 1256–1263. https://doi.org/10.4319/lo.1978.23.6.1256

Sigman, D. M., Casciotti, K. L., Andreani, M., Barford, C., Galanter, M., & Böhlke, J. K. (2001). A bacterial method for the nitrogen isotopic analysis of nitrate in seawater and freshwater. *Analytical Chemistry*, *73*(17), 4145–4153. https://doi.org/10.1021/ac010088e

Sohm, J. A., Webb, E. A., & Capone, D. G. (2011). Emerging patterns of marine nitrogen fixation. *Nature Reviews Microbiology*, *9*(7), 499–508. https://doi.org/10.1038/nrmicro2594

Sweeney, E. N., McGillicuddy, D. J., & Buesseler, K. O. (2003). Biogeochemical impacts due to mesoscale eddy activity in the Sargasso Sea as measured at the Bermuda Atlantic Time-series Study (BATS). *Deep-Sea Research II*, *50*(22–26), 3017–3039. https://doi.org/10.1016/j.dsr2.2003.07.008

Uitz, J., Claustre, H., Morel, A., & Hooker, S. B. (2006). Vertical distribution of phytoplankton communities in open ocean: An assessment based on surface chlorophyll. *Journal of Geophysical Research*, *111*(8), C08005. https://doi.org/10.1029/2005JC003207

Vaillancourt, R. D., Marra, J., Seki, M. P., Parsons, M. L., & Bidigare, R. R. (2003). Impact of a cyclonic eddy on phytoplankton community structure and photosynthetic competency in the subtropical North Pacific Ocean. *Deep-Sea Research I*, *50*(7), 829–847. https://doi.org/10.1016/S0967-0637(03)00059-1

Van Mooy, B. A. S., Fredricks, H. F., Pedler, B. E., Dyhrman, S. T., Karl, D. M., Koblížek, M., et al. (2009). Phytoplankton in the ocean use non-phosphorus lipids in response to phosphorus scarcity. *Nature*, *458*(7234), 69–72. https://doi.org/10.1038/nature07659

Wan, X. S., Sheng, H. X., Dai, M., Zhang, Y., Shi, D., Trull, T. W., et al. (2018). Ambient nitrate switches the ammonium consumption pathway in the euphotic ocean. *Nature Communications*, *9*(1), 1–9. https://doi.org/10.1038/s41467-018-03363-0

Wang, L., Huang, B., Laws, E. A., Zhou, K., Liu, X., Xie, Y., & Dai, M. (2018). Anticyclonic eddy edge effects on phytoplankton communities and particle export in the northern South China Sea. *Journal of Geophysical Research: Oceans*, *123*(11), 7632–7650. https://doi.org/10.1029/2017JC013623

Ward, B. A., Dutkiewicz, S., Moore, C. M., & Follows, M. J. (2013). Iron, phosphorus, and nitrogen supply ratios define the biogeography of nitrogen fixation. *Limnology and Oceanography*, *58*(6), 2059–2075. https://doi.org/10.4319/lo.2013.58.6.2059

Wen, Z., Browning, T. J., Cai, Y., Dai, R., Zhang, R., Du, C., et al. (2022). Nutrient regulation of biological nitrogen fixation across the tropical western North Pacific. *Science Advances*, *8*(5), 7564. https://doi.org/10.1126/SCIADV.ABL7564

White, A. E., Spitz, Y. H., Karl, D. M., & Letelier, R. M. (2006). Flexible elemental stoichiometry in Trichodesmium spp. and its ecological implications. *Limnology and Oceanography*, *51*(4), 1777–1790. https://doi.org/10.4319/lo.2006.51.4.1777

Wilson, S. T., Aylward, F. O., Ribalet, F., Barone, B., Casey, J. R., Connell, P. E., et al. (2017). Coordinated regulation of growth, activity and transcription in natural populations of the unicellular nitrogen-fixing cyanobacterium Crocosphaera. *Nature Microbiology*, *2*(9), 17118. https://doi.org/10.1038/NMICROBIOL.2017.118

Wilson, S. T., Böttjer, D., Church, M. J., & Karl, D. M. (2012). Comparative assessment of nitrogen fixation methodologies, conducted in the oligotrophic North Pacific Ocean. *Applied and Environmental Microbiology*, *78*(18), 6516–6523. https://doi.org/10.1128/AEM.01146-12

Wu, J., Sunda, W., Boyle, E. A., & Karl, D. M. (2000). Phosphate depletion in the western North Atlantic Ocean. *Science*, *289*(5480), 759–762. https://doi.org/10.1126/science.289.5480.759

Yuan, Z., Browning, T. J., Zhang, R., Wang, C., Du, C., Wang, Y., et al. (2023). Potential drivers and consequences of regional phosphate depletion in the western subtropical North Pacific. *Limnology and Oceanography Letters*, *8*(3), 509–518. https://doi.org/10.1002/lol2.10314

Yuan, Z., & Dai, M. (2023). Experimental dataset for 'Enhanced phosphate consumption stimulated by nitrogen fixation within a cyclonic eddy in the Northwest Pacific' [Dataset]. Science Data Bank. https://doi.org/10.57760/sciencedb.08040

Yun, M. S., Kim, Y., Jeong, Y., Joo, H. T., Jo, Y. H., Lee, C. H., et al. (2020). Weak response of biological productivity and community structure of phytoplankton to mesoscale Eddies in the Oligotrophic Philippine Sea. *Journal of Geophysical Research: Oceans*, *125*(12), e2020JC016436. https://doi.org/10.1029/2020JC016436

Zehr, J. P., & Capone, D. G. (2020). Changing perspectives in marine nitrogen fixation. *Science*, *368*(6492), eaay9514. https://doi.org/10.1126/science.aay9514

Zehr, J. P., & Capone, D. G. (2021). *Marine nitrogen fixation*. Springer.

Zhang, J. Z. (2000). Shipboard automated determination of trace concentrations of nitrite and nitrate in oligotrophic water by gas-segmented continuous flow analysis with a liquid waveguide capillary flow cell. *Deep-Sea Research I*, *47*(6), 1157–1171. https://doi.org/10.1016/S0967-0637(99)00085-0

Zhang, Z., & Qiu, B. (2020). Surface chlorophyll enhancement in mesoscale eddies by submesoscale spiral bands. *Geophysical Research Letters*, *47*(14), e2020GL088820. https://doi.org/10.1029/2020GL088820

Zhou, K., Dai, M., Xiu, P., Wang, L., Hu, J., & Benitez-Nelson, C. R. (2020). Transient enhancement and decoupling of carbon and opal export in cyclonic eddies. *Journal of Geophysical Research: Oceans*, *125*(9), 1–17. https://doi.org/10.1029/2020JC016372

Zhou, K., Xu, Y., Kao, S. J., Xiu, P., Wan, X., Huang, B., et al. (2023). Changes in nutrient stoichiometry in responding to diatom growth in cyclonic eddies. *Geoscience Letters*, *10*(1), 1–12. https://doi.org/10.1186/s40562-023-00269-8